European Journal of Forest Research
https://doi.org/10.1007/s10342-024-01734-5

RESEARCH

Exploring forest changes in an *Ips typographus* L. outbreak area: insights from multi-temporal multispectral UAS remote sensing

Madeleine Östersund[1,2] · Eija Honkavaara[1] · Raquel A. Oliveira[1] · Roope Näsi[1] · Teemu Hakala[1] · Niko Koivumäki[1] · Mikko Pelto-Arvo[3] · Johanna Tuviala[3] · Olli Nevalainen[4] · Päivi Lyytikäinen-Saarenmaa[1,3]

Received: 31 December 2023 / Revised: 24 August 2024 / Accepted: 27 September 2024
© The Author(s) 2024

Abstract

Uncrewed Aerial Systems (UAS) offer a versatile solution for monitoring forest ecosystems. This study aimed to develop and assess an individual tree-based methodology using multi-temporal, multispectral UAS images to track changes caused by the European spruce bark beetle (*Ips typographus* L.). The approach encompassed four key steps: (1) individual tree detection using structure-from-motion point clouds, (2) tree species classification, (3) health classification of spruce trees as healthy, declined, or dead, and (4) change detection, identifying fallen/removed trees and alterations in tree health status. The developed methodology was employed to quantify changes in a bark beetle outbreak area covering 215 hectares in southeastern Finland during 2019–2021. The dataset included two managed and two conserved forest areas. The uncertainty estimation demonstrated the overall accuracies ranging from 0.58 to 0.91 for individual tree detection, 0.84 for species classification, and 0.83–0.96 for health classification, and a F1-score of 0.91 for the fallen or removed tree detection. Maps and statistics were produced, containing information on the health of the spruce trees in the area and information on changes, including trees that died during monitoring and those that fell or were removed from the forest. The results demonstrated successful control of the outbreak in the managed stands, evidenced by moderate tree mortality. Conversely, in the conserved stands, the outbreak resulted in dramatic tree mortality. This method serves stakeholders by enabling large-scale outbreak impact monitoring, facilitating timely risk assessment, and validating bark beetle outbreak management strategies.

Keywords UAS · Bark beetle · Remote sensing · Multi-temporal · Machine learning · Change

Communicated by Lauri Mehtätalo.

✉ Eija Honkavaara
eija.honkavaara@nls.fi

Madeleine Östersund
madeleine.c.ostersund@uit.no

Raquel A. Oliveira
raquel.alvesdeoliveira@nls.fi

Roope Näsi
roope.nasi@nls.fi

Teemu Hakala
teemu.hakala@nls.fi

Niko Koivumäki
niko.koivumaki@nls.fi

Mikko Pelto-Arvo
mikko.pelto-arvo@uef.fi

Johanna Tuviala
johanna.tuviala@uef.fi

Olli Nevalainen
olli.nevalainen@fmi.fi

Päivi Lyytikäinen-Saarenmaa
paivi.lyytikainen-saarenmaa@uef.fi;
paivi.lyytikainen-saarenmaa@nls.fi

[1] Department of Remote Sensing and Photogrammetry, Finnish Geospatial Research Institute in National Land Survey of Finland (FGI), 02150 Espoo, Finland

[2] Department of Physics and Technology, UiT The Arctic University of Norway, 9019 Tromsö, Norway

[3] School of Forest Sciences, University of Eastern Finland, 80100 Joensuu, Finland

[4] Climate System Research, Finnish Meteorological Institute, 00560 Helsinki, Finland

Published online: 09 October 2024

Introduction

Boreal forests in central and northern Europe are threatened by biotic and abiotic stresses at an increasing rate as a consequence of climate change (Patacca et al. 2023; Barrere et al. 2023). The risk of outbreaks by the European spruce bark beetle (*Ips typographus* L.) has increased in Norway spruce (*Picea abies* L.) stands. At normal circumstances, the bark beetle improves the biodiversity in the forest, composing small gaps and increasing a mosaic structure of a forest. However, a trend of earlier spring and warmer summer months since the 1990s, have increased the outbreaks rapidly as defense mechanisms of the spruces weaken due to dry spells. Even if the role of the bark beetle is debatable in conserved forests, it evidently causes a threat to diversity and ecosystem services of stands, and to economic value in managed forests at a gradation peak (Hlásny et al. 2021).

The analysis of forest disturbances through field inspections is laborious and expensive, making it unsuitable for covering large areas (Barta et al. 2022). There is thus a great relevance to develop remote sensing techniques that offer cost-efficient mapping possibilities (Rhodes et al. 2022). While optical satellite remote sensing has proven to be a powerful tool for monitoring large areas, its spatial resolution does not reach the individual tree level, and datasets are only accessible under cloud-free conditions. In contrast, Uncrewed Aerial Systems (UAS) equipped with high-resolution remote sensing cameras, combined with machine learning (ML) based data analysis, offer a highly promising and advanced approach for monitoring forest conditions at the individual tree level (Sun et al. 2021; Ecke et al. 2022; Rhodes et al. 2022).

UAS remote sensing methods have proven to be effective in analyzing bark beetle infestations (Ecke et al. 2022). The methods are based on the study of the crown discoloration symptoms that occur when the transport of water and nutrients in the tree is disturbed. As the infestation progresses, the color of the crown changes from green to yellow, red-brown and finally gray when the tree dies completely (Barta et al. 2022). The first stage of infestation, when the signs of the attack, such as entrance holes, resin flows, and boring dust, are already visible on the trunk but the crown is still green, is called the "green attack" stage (Huo et al. 2023). Previous studies have shown that the advanced, visible crown color symptoms, can be detected with a good accuracy, with F1-scores ranging from 0.80 to 0.9 and above, using a variety of technologies, including color (RGB) cameras (Safonova et al. 2022; Kanerva et al. 2022), multispectral cameras (Fraser and Congalton 2021; Minarik et al. 2021; Junttila et al. 2022; Huo et al. 2023) or hyperspectral cameras (Honkavaara et al. 2020; Turkulainen et al. 2023). Outcomes of forest health analysis during an outbreak are tree health maps, where individual spruce trees are detected and given health classes (e.g., Junttila et al. 2022).

Analysis of forest health at one point in time gives valuable information on the state of the forest, but multi-temporal data gives an overview of the declining and disturbance spreading process. A previous review by Ecke et al. (2022) promoted the value of multi-temporal analysis in forest disturbance analysis, but at the same time showed that the scientific literature on this field is still limited and highlighted the importance of further research on the topic. In the case of bark beetle outbreak monitoring, studies using multi-temporal datasets have investigated how and when spruces start showing spectral differences after the infestation (Honkavaara et al. 2020; Huo et al. 2023) and studied ideal season for detecting decline (Junttila et al. 2022; Klouček et al. 2019). The multi-temporal analysis has improved detection of pine wilt disease, which is another serious tree-killing biotic disturbance (Wu et al. 2021; Yu et al. 2021). Furthermore, Dash et al. (2017) demonstrated the feasibility of temporal monitoring in a case of simulated disturbance. Multi-temporal UAS imagery has shown promising results in challenging combined species and health analysis tasks (Michez et al. 2016; Abdollahnejad and Panagiotidis 2020; Grybas and Congalton 2021), which will become relevant when analyses are expanded over larger areas. Recent studies have also shown feasibility of multi-temporal UAS images and point clouds in analysis of vegetation dynamics and disturbance monitoring (Dandois and Ellis 2013; Guerra-Hernández et al. 2017; Araujo et al. 2021), phytosanitary analysis (Pádua et al. 2017), and drought stress detection (D'Odorico et al. 2021). Studies have thus far mostly used data from one season. Multi-temporal data covering several years, however, could enable analysis and enhance our understanding of the outbreak dynamics and spreading.

Studies on multi-temporal UAS-based monitoring of bark beetle outbreak areas have focused on analysis of health status of standing spruce trees and have not analysed other aspects of forest ecosystem such as structural changes and fallen trees. For structural analysis, 3D point clouds can be produced using Light Detection and Ranging (LiDAR) (Lefsky et al. 1999; Næsset 2002; Liang et al. 2022) or photogrammetric structure-from-motion (SfM) techniques (Iglhaut et al. 2019). In this study, multi-temporal photogrammetric point clouds were used to detect tree crown losses in the forest. The photogrammetric approach is cost-effective when UAS images are needed for health analysis, as in such cases, the images and point clouds can be produced with a single sensor. Photogrammetric point clouds have demonstrated good performance in structural analysis (Dandois and Ellis 2013; Araujo et al. 2021; Nuijten et al. 2021), although LiDAR based approaches have outperformed SfM in

structural analysis (Ramalho De Oliveira et al. 2020; Chung et al. 2022). The predominant reasons for tree crown loss during bark beetle outbreaks are generally associated with tree falls due to death or tree removal as part of forest management operations. Fallen trees laying on ground can be detected using image-based techniques (Panagiotidis et al. 2019; Thiel et al. 2020; Polewski et al. 2021) or through the use of LiDAR (Polewski et al. 2015; Heinaro et al. 2023).

The objective of this study was to develop an individual tree-level methodology for monitoring changes in a forest ecosystem using a remote sensing-based approach with multi-temporal multispectral UAS images. The method was applied to investigate the disturbances in a bark beetle outbreak area in Southeast Finland, using imagery collected in August of 2019, 2020, and 2021. The study aimed to address two major research questions: (1) What is the performance of the proposed methodology? (2) What insights does the UAS-based method provide regarding the development of the outbreak in managed and conserved forests?

Materials and methods

Overview of the methodology

The proposed UAS remote sensing approach for outbreak monitoring consists of two major phases: data capture and data analysis (Fig. 1). Data capture involves UAS data capture flights as well as subsequent photogrammetric processing steps to produce point clouds, canopy height models (CHM), and orthomosaics. Additionally, in situ references are collected to facilitate the implementation and validation of supervised ML methods. The proposed data analysis pipeline comprises five major steps: (1) tree detection, (2) image feature extraction, (3) species classification, (4) tree health estimation, and (5) change detection and analysis including fallen tree detection and spruce tree health change detection. In the first step, UAS point clouds are used to detect trees. Following this, features are extracted from the multispectral images for subsequent remote sensing analysis tasks. In the third step, tree species classification is performed using multispectral features to identify spruce trees susceptible to bark beetle attacks. The fourth step determines the health classes of the detected spruce trees. In the final step, forest changes are identified by detecting fallen/removed trees and comparing tree health maps from different years. This process generates maps and statistics, providing insights into the impacts and changes within the area.

The proposed approach for the continuous monitoring in a practical application (as sketched in Fig. 1) involves conducting tree detection and species classification using data from the first year to identify the initial state of the forest ecosystem. Datasets from the subsequent years are then used for health classification of spruce trees and change analysis.

Study area and field reference capture

The study area was a multiyear monitoring site for the European spruce bark beetle (*Ips typographus* L.) in Ruokolahti, Finland (61°29′ 21.840″ N, 29°3′ 0.720″ E) (Fig. 2). The area was hit by a serious summer storm in 2010 and a bark beetle outbreak initiated four years later in standing trees. Since 2014, populations showed a fluctuating and sporadic nature, depending on prevailing weather conditions (see

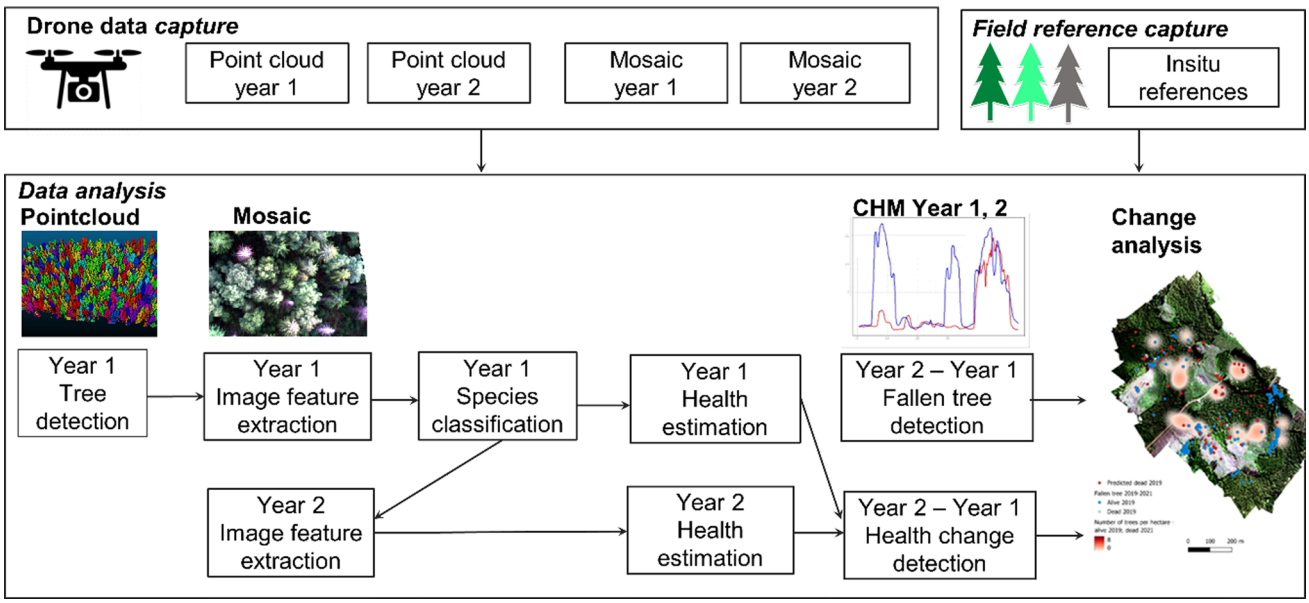

Fig. 1 Methodology for tree health monitoring from multi-temporal UAS datasets

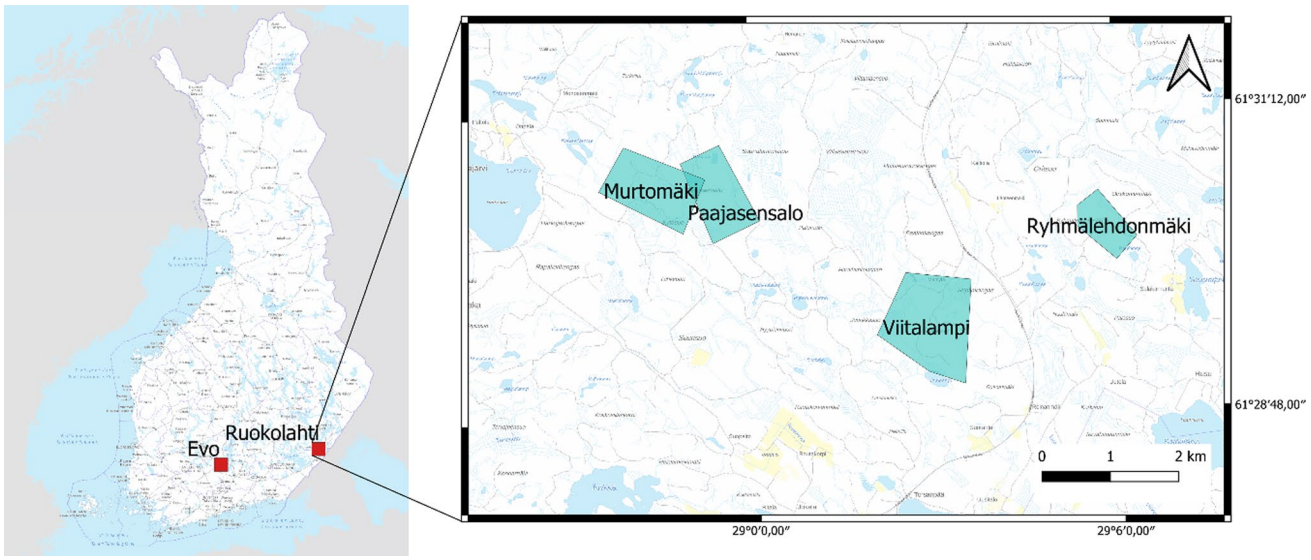

Fig. 2 Location of the study sites in Ruokolahti 2019–2021 and Evo 2018. Background map (raster) from Finnish National Land Survey (NLS) 09/11/2023 https://www.maanmittauslaitos.fi/en/opendata-licence-cc40

Kosunen et al. 2019). Temperature of summer months in 2018 was high and precipitation low, promoting reproduction of *I. typographus*. However, clusters of dead and clearly declined trees were still quite small in 2019–2021. The reference data was collected in four study sites: Murtomäki, Paajasensalo, Ryhmälehdonmäki, and Viitalampi. Of these sites, Paajasensalo and Viitalampi are nature conservation areas, while Ryhmälehdonmäki and Murtomäki are managed forests. All the study sites are dominated by mature Norway spruce trees (Table 1).

Bark beetle symptom field data was collected late in the summer during 2019–2021. In total, 66 circular sample plots were measured by forest experts. Each sample plot had a radius of 10 m and included 10–30 trees. The center coordinate of each plot was measured using a Trimble Geo TX GPS-device (Trimble Navigation Ltd., Sunnyvale, CA, USA) and the surrounding trees were located measuring the distance and azimuth from the plot center. For each tree, tree species, height, diameter at breast height (DBH), and the health status were recorded (Table 1). The age was measured for every seventh spruce across the plots. Suppressed trees with a height of less than 10 m and a DBH of less than 10 cm were ignored. Also, potential fallen trees were identified. Tree health data was collected by experts evaluating various symptoms and their severity levels (Table 2). The bark beetle symptom categories were crown discoloration, defoliation, bark damage, resin flow, and entrance and exit holes. Each symptom was rated with 3–4 different scores based on the symptom severity. More details about the health evaluation procedure can be found from Blomqvist et al. (2018).

Field measurements indicated a significant number of dead spruce trees, attributed to a strong earlier colonization pressure. The proportion of recently infested reference trees showing discoloration symptoms was small due to a

Table 1 Main parameters of the trees (height ≥ 10 m, DBH ≥ 10 cm) on plots in each study site

Study site	Year		Study site parameters				Species composition (%)		
			Age (years)	DBH (cm)	Height (m)	N Trees/ha	Spruce	Deciduous	Pine
Paajasensalo	2019	Ave	127.52	22.24	18.75	555	89	4	7
		Sd	±48.31	±7.61	±4.77	±150			
Viitalampi	2019	Ave	96.97	24.47	21.10	407	86	11	3
		Sd	±28.20	±8.88	±5.54	±195			
Ryhmä-lehdonmäki	2019	Ave	47.40	23.99	20.33	500	92	3	5
		Sd	±6.47	±6.20	±3.67	±94			
Murtomäki	2019	Ave	48.63	21.93	19.41	668	98	2	1
		Sd	±7.32	±6.04	±3.37	±146			

Ave: average; Sd: standard deviation

Table 2 Bark beetle infestation symptoms and the different classes given to describe the health status of a spruce tree (adopted and adapted from Blomqvist et al. 2018)

Symptom	Class	Description
Number of resin flows	1	< 2
	2	2–30
	3	> 30 spots
Number of entrance and exit holes	1	< 2
	2	Mild infestation (2–10)
	3	Severe infestation (> 10)
Bark	1	Healthy
	2	Minor damage
	3	Major damage
Discoloration	1	Healthy, green
	2	Yellowish
	3	Reddish
	4	Dead, gray
Defoliation	1	0–25%
	2	26–50%
	3	51–75%
	4	76–100%

The number of entrance and exit holes indicate the case up to 2 m height

surpassed outbreak peak. While the majority of reference trees exhibited green crowns, a considerable number of these green trees displayed trunk symptoms, attributed to either low population densities or an early phase of colonization. The multi-year dataset revealed that many trees with low or moderate stem symptoms managed to recover from the attack, possibly due to higher resistance or a low population density.

An additional dataset from a different location, Evo, Finland (61°10′ 19.835″ N, 25°8′ 7,808″ E) (Fig. 2), was used to increase the amount of tree species training data. The dataset included four forest plots of size 20 m by 20 m with individual tree species information (spruce, pine and birch). In this study, species information of dominant and co-dominant trees that were visible in the aerial images was used to increase training data for species classification. Details of the forest area are described by Liang et al. (2018). Furthermore, 150 additional not-spruce trees were visually selected from the orthomosaics to increase the number of not-spruce trees.

The dataset was further filtered so that trees less than 10 m tall were removed from the dataset. These trees were most likely suppressed trees. Furthermore, previous results have shown that bark beetles attack spruces with a DBH of minimum 10 cm (Kärvemo et al. 2014; Müller et al. 2022) that corresponds to tree height of 10 m in the test area. The coordinates of the reference trees did not perfectly align with the remote sensing datasets collected from the area due to the challenges of global navigation satellite system (GNSS) based positioning inside forest. To address this, the coordinates of the trees were refined by using orthoimages to match the remote sensing data. An overview of the filtered set of reference trees is presented in Table 3.

UAS datasets

UAS data acquisition in Ruokolahti bark beetle monitoring site was carried out at the end of the summer season in August in each year (Table 4). Multispectral image data was captured using a Micasense Altum (AgEagle Aerial Systems Inc., Wichita, KS, USA) camera, which included bands in the blue (central wavelength: 475 nm), green (560 nm), red (668 nm), red-edge (717 nm), and near-infrared (842 nm) spectral range. The flight height was around 140–150 m resulting in a ground sample distance (GSD) of 6–8 cm (Table 4). Images were pre-processed into point-clouds and multispectral orthomosaics using SfM techniques with

Table 3 The number of reference trees (height ≥ 10 m, DBH ≥ 10 cm) used from each study site, discoloration class of spruces and number of other species

Study site	Year	Spruce	Not-spruce				
		Green	Yellowish	Reddish	Grey	Deciduous	Pines
Paajasensalo	2019	52	5	0	39	11	10
	2020	56	1	0	39	11	10
	2021	51	5	1	39	11	10
Viitalampi	2019	151	1	0	110	32	11
	2020	149	3	0	110	32	11
	2021	143	7	0	112	32	11
Ryhmälehdonmäki	2019	51	0	0	0	0	4
	2020	51	0	0	0	0	4
	2021	48	3	0	0	0	4
Murtomäki	2019	110	0	0	0	1	1
	2021	110	0	0	0	1	1
Evo	2018	126	0	0	0	44	128

Table 4 Details of the remote sensing datasets

Dataset	Date	Area (ha)	Weather	FA (m)	GSD (cm)	Equipment
MM_2019	28.8.2019	60	Sunny	140	6	Altum Quadcopter
MM_2021	31.8.2021	90	Varying	150	7	Altum, DJI Matrice 300 RTK
PS_2019	28.8.2019	45	Sunny	140	6	Altum, Quadcopter
PS_2020	27.8.2020	32	Varying	140	6	Altum, Quadcopter
PS_2021	31.8.2021	75	Varying	140	6	Altum, DJI Matrice 300 RTK
RM_2019	27.8.2019	27	Sunny	140	6	Altum, Quadcopter
RM_2020	27.8.2020	20	Sunny	140	6	Altum, Quadcopter
RM_2021	30.8.2021	45	Varying	150	7	Altum, DJI Matrice 300 RTK
VL_2019	27.–28.8.2019	120	Sunny	140	8	Altum, Quadcopter
VL_2020	27.8.2020	80	Varying	140	6	Altum, Quadcopter
VL_2021	30.8.2021	120	Varying	150	7	Altum, DJI Matrice 300 RTK
Evo_2018 1002	3.8.2018	6	Varying	120	8	Red Edge, Quadcopter
Evo_2018 1009	8.8.2018	5	Sunny	120	7	Red Edge, Quadcopter
Evo_2018 1014	3.8.2018	5	Sunny	120	8	Red Edge, Quadcopter
Evo_2018 1060	8.8.2018	6	Varying	120	7	Red Edge, Quadcopter

FA: Flying altitude; GSD: Ground Sample Distance; MM: Murtomäki, PS: Paajasensalo, RM: Ryhmälehdonmäki, VL: Viitalampi

Agisoft Metashape software (Agisoft LLC, St. Petersburg, Russia) following the procedure described by Nevalainen et al. (2017). For the 2021 Altum images, the precise real-time kinematic (RTK) GNSS positioning was available. For the 2019–2020 datasets, ground control points (GCPs) were placed in 4–8 locations in each area and measured using the RTK GNSS receiver (Topcon Hiper HR; Topcon, Tokyo, Japan) with an expected accuracy of 0.03–0.05 m. However, the accuracy of GNSS measurements in a forested environment might be reduced due to limited satellite visibility. Therefore, additional GCPs extracted from existing orthomosaics of the area were used whenever needed to support georeferencing. Radiometric calibration into reflectance values was conducted using the panel provided by Micasense.

The orthomosaics from 2019 and 2020 required an additional geometric processing to accurately align them with the orthomosaics of 2021. This process used the 'georeferencer' plugin in QGIS (QGIS.ORG, Grüt, Switzerland) with a 2nd order polynomial transformation. This additional image transformation was necessary due to geometric mismatches between orthomosaics from different years that could potentially disrupt change analysis. The 2021 dataset had an accurate georeferencing because the UAS had precise RTK GNSS positioning onboard. In the 2019 and 2020 datasets, there were a small number of GCPs that possibly had reduced accuracy due to difficulties of GNSS positioning inside the forest caused by limited satellite visibility.

The Evo data, utilised for species classification, was captured in early August 2018 with a Micasense Red Edge camera that had similar spectral characteristics as the Altum camera. The data was processed similarly to the datasets from Ruokolahti.

Procedure for forest plot analysis

Tree detection

The local maximum algorithm (FUSION version 4.21, US Department of Agriculture, Forest Service, Pacific Northwest Research Station; Nevalainen et al. 2017) was used to detect all trees from the CHMs calculated by subtracting the national digital terrain model (DTM 2 m) data from the UAS point cloud produced using the SfM method. The DTM 2 m is produced by the National Land Survey of Finland (NLS) using the laser scanning datasets of the national topographic data production program and is openly available. Detected suppressed trees with a height under 10 m were ignored as they were not considered at risk of the bark beetle attack (Kärvemo et al. 2014; Müller et al. 2022). Additionally, trees close to orthomosaic edges were ignored and trees with several maxima were filtered so that each tree was represented by one point. As the local maximum algorithm is a direct method for tree detection, without involving ML, reference tree data could be utilised as independent test data to assess the performance of the tree detection.

Image feature extraction and machine learning

The coordinates of the reference trees, and the detected trees were used to extract features from the multispectral images to be used as explanatory variables in the subsequent ML

analysis. The features included spectral values and vegetation indices (VIs) for each individual tree.

The features were calculated as an average of all pixels within a circle with 1 m diameter, centered at the position of the detected treetop. The spectral band features of the five bands were normalised using the spectral feature length (Euclidean distance) to reduce the effect of illumination and other differences between the years; the normalization compensated for well these differences and the spectral data of different datasets were highly consistent (Fig. 4, Appendix A). The following 24 VIs were calculated: ARVI (Atmospherically Resistant Vegetation Index), ARVI 2, BNDVI (Blue Normalized Difference Vegetation Index), CI (Chlorophyll Index), CIG (Chlorophyll Index-Green), CVI (Chlorophyll Vegetation Index), DATT1 (Estimation of chlorophyll content), DATT6, ExG (Excess Green), ExGR (Excess Green minus Excess Red), ExR (Excess Red), GLI (Green Leaf Index), GNDVI (Green Normalized Difference Vegetation Index), LogR (Logarithmic Ratio), MTVI (Modified Triangular Vegetation Index), NDRE (Normalized Difference Red Edge), NDVI (Normalized Difference Vegetation Index), OSAVI (Optimized Soil Adjusted Vegetation Index), RDVI (Renormalized Difference Vegetation Index), RE1 (Red Edge), RGBVI (Red–Green–Blue Vegetation Index), RGBVI2, SAVI (Soil Adjusted Vegetation Index), TCI (Temperature Condition Index). Equations of different indices are given in Table 11 (Appendix B).

Random Forest (RF) (Breiman 2001) ML method was used to train the classifiers, considering its successful performance in similar use cases (Nevalainen et al. 2017; Abdollahnejad and Panagiotidis 2020; Hartling et al. 2021; Junttila et al. 2022). The main parameters of the RF (number of trees; criterion, i.e., the quality of a split in each decision tree; maximum tree depth; maximum features; class weight) were fine-tuned using a grid search method (Bergstra and Bengio 2012). Three different feature selection methods were compared: using all features, K-best, and RF-recursive features. K-best selects the *k* features (in this case, 5) based on Analysis of Variance (ANOVA) and eliminates all others. Recursive feature selection ranks the features by the importance computed for the ML algorithm (Pedregosa et al. 2011). The training data was divided into training (80%) and validation (20%) datasets for parameter tuning. Both VIs and normalised spectral features were used as input features. The described ML method was implemented using the python module Scikit-learn (Pedregosa et al. 2011).

Tree species classification

Trees were classified into three classes: not-spruce trees (deciduous and pine trees), spruce trees, and dead spruce trees. The ML model for species classification was trained using the tree species reference data from Ruokolahti (Viitalampi: 2019, 2020; Murtomäki: 2020; Ryhmälehdonmäki: 2019, 2020; Paajasensalo: 2020) and Evo. From Ruokolahti, datasets from 2019 and 2020 were used, as these datasets had consistent reflectance values. The Paajasensalo 2019 dataset from Ruokolahti was used as an independent test data for evaluating the performance of the classifier. Only those reference trees that were considered as detected in the tree detection phase (when using the 1 m criteria for reference and detected tree top positions) were used to reduce the effect of off-centered coordinates. The final numbers of reference trees were 325 spruce trees, 265 not-spruce trees, and 126 dead spruce trees.

RF was used to train the species classifier model as described in Section "Image feature extraction and machine learning". After training, the species classification was done for the multispectral orthophotos from 2019 to provide species information for the detected trees over the entire study area.

Spruce tree health classification

Spruce tree health classification was carried out using two symptom rules that were based on the health indexes calculated based on the spruce tree symptom observations (Table 2): one based on crown color symptoms (Eq. 1), and one based on both crown and trunk symptoms (Eq. 2), symptom rules 1 and 2, respectively.

$$\text{Health index 1} = \textit{Discoloration} \tag{1}$$

$$\text{Health index 2} = 1.5(\textit{Discoloration} + \textit{Defoliation}) + \textit{Resin flow} + \textit{Bark damage} \tag{2}$$

Based on the health index, three classes "Healthy", "Declined" and "Dead" were defined. The health index 1 is commonly used when analyzing bark beetle outbreaks (e.g., Näsi et al. 2015; 2018; Minarik et al. 2021; Safonova et al. 2022). The health index 2 was initially proposed by Junttila et al. (2022) while Kanerva et al. (2022) studied the use of health indices 1 and 2 using RGB images. For the symptom rule 1, the health index value of 1 was considered as healthy, of 2 and 3 as declined, and of 4 as dead. For the symptom rule 2, the health index values of 5–7.5 were considered as healthy, of 7.5–14 as declined, and of 14–18 as dead. The resulting numbers of reference trees were 664 healthy, 17 declined, and 284 dead spruce trees for the symptom rule 1, and 405 healthy, 281 declined, and 284 dead spruce trees for the symptom rule 2.

The RF method was used to train the spruce tree health classifier model, as described in Section "Image feature extraction and machine learning". The reference trees from Ryhmälehdonmäki, Viitalampi, and Murtomäki from the years 2019, 2020, and 2021 were used as training data, while

the Paajasensalo datasets were used as independent test data to ensure reliable performance assessments. After training the classifier, the spruce trees detected in each test area were classified into different health classes.

Change analysis

Change analysis included fallen/removed tree detection and the analysis of tree health change.

In this study, we did not specifically analyze the reasons for trees' disappearance from the forest. Potential causes include the death and falling of the tree due to bark beetle infestation or intentional felling and removal as part of forest management. Fallen/removed trees were detected by comparing changes in CHMs from 2019 and 2021. A CHM raster difference layer (ΔCHM) was created using raster calculation in QGIS:

$$\Delta CHM = CHM_{2019} - CHM_{2021}. \quad (3)$$

At the start of the monitoring, standing trees were identified using point clouds from the 2019 dataset, following the methodology outlined in Section "Tree detection". Subsequently, change detection analysis was applied to these identified trees. Firstly, a tree was considered fallen/removed if the mean ΔCHM within a 1 m radius of the tree position was larger than 5 m. Due to the characteristics of the photogrammetric point clouds, several additional filtering steps were necessary. SfM technique provided high point densities for tree crowns in all datasets because they were well illuminated and had suitable textures and thus were well suited for image matching. However, in shady forest gaps where fallen/removed trees were located, the point clouds often had imperfections, manifested as lower point densities and noise. Furthermore, the point densities were lower in the 2019 dataset than in the 2021 dataset. To account for the areas with incomplete point clouds, a raster of point density layer with 1 m×1 m resolution was generated for each dataset using the 'Lasgrid' function from LASTools (version 210,720) (rapidlasso GmbH, Gilching, Germany). In 2019 dataset, trees that had a mean point density less than 30 points/m^2 were considered as low-quality point clouds and were disregarded from analysis. Next, considering the imperfections of point clouds in the forest gaps and differences in point cloud quality across different years, two criteria were considered using the point density raster: (a) trees that had the mean point density less than 80 points/m^2 in the 2021 point cloud and (b) trees having significantly higher (> 1.5 times higher) point cloud density in the 2019 dataset than in the 2021 dataset were considered as fallen/removed trees. These limits were selected by visual analysis of datasets.

Since the proposed method directly identified missing crowns from the point clouds, fallen/removed trees between 2019 and 2021 in the reference data served as independent ground truth for performance assessment. Only trees taller than 10 m were considered in the reference data to align with the detected tree data.

To study the development of the outbreak, the changes that occurred in the spruce health classes between 2019 and 2021 were analysed. The focus of this analysis was to understand how the outbreak has spread, using the appearance of newly dead trees as an indicator of the outbreak's expansion. This analysis was conducted using the 'Kernel Density' heatmap analysis in QGIS.

Performance assessment

Performance of each phase of the process was evaluated using independent test data followed by calculating descriptive statistics, including precision, recall, F1-score and overall accuracy (OA). Precision represents the ratio between correctly predicted values and the total number of predicted values in that class:

$$precision = \frac{TP}{(TP + FP)}, \quad (4)$$

where TP is true positives and FP is false positives.

Recall represents the correctly predicted fraction of the ground truth as

$$recall = \frac{TP}{(TP + FN)}, \quad (5)$$

where FN is false negatives.

Precision and recall are inversely related metrics. As the precision increases, the recall typically decreases, and vice versa. The F1-score provides a measure of the optimal balance between these two metrics and is calculated as the harmonic mean value of precision and recall:

$$F1 - score = 2 \cdot \frac{precision \cdot recall}{precision + recall}. \quad (6)$$

OA is calculated by dividing the number of correctly predicted values with the total number of values as.

$$OA = \frac{TP + TN}{TP + FP + TN + FN}. \quad (7)$$

In this context, it is important to note that the performance of each stage was assessed using independent test data. ML was not employed in tree detection and fallen tree detection, and therefore, the reference datasets served as independent test data. For assessing ML models of species and tree health classification, one of the test areas was excluded from the training set and used as unseen test data. For tree detection, OA was computed by verifying whether a reference tree was found within a radius of 1 m from the detected treetop (Section "Tree detection"). The tree species classification model's performance was assessed

using the Paajasensalo 2019 dataset (Section "Tree species classification") and to assess the performance of the tree health classification models, the Paajasensalo datasets were utilised (Section "Spruce tree health classification"). Fallen/removed tree detection performance was evaluated using the fallen trees present in the field measured dataset (Section "Change analysis").

Results

Remote sensing method development

Tree detection

Table 5 displays the number of reference trees, the number of detected reference trees, the achieved OA, and the total number of detected trees for each area. Ryhmälehdonmäki had the best results with an OA of 0.91, and Murtomäki had the second-best OA of 0.74; these areas were the managed forests and potentially had better separation of individual trees. Results in the conserved forests were poorer, with an OA of 0.58–0.70. It is likely that many of the smaller reference trees were hidden under dominating trees. The combined OAs were 0.80 for managed forests, 0.61 for conserved forests, and 0.66 for all areas. Also, it is possible that the distance limit between a detected tree and its reference tree should have been larger than the 1 m radius used in this study.

Tree species classification

For the tree species classification model, the OA was 0.84 for the training validation dataset and 0.89 for the independent Paajasensalo 2019 testing dataset (Table 6). F1-scores were 0.86, 0.83, and 1.00 for not-spruce, spruce, and dead spruce classes, respectively, in the independent test data. The confusion matrix and statistics evaluation indicated that the healthy and dead spruce trees were correctly classified, but that some of the not-spruce trees were misclassified as spruce trees (Table 7).

The parameter tuning provided the following parameters for the RF classifier model: *Number of trees*: 100; *Criterion:* entropy; *Maximum depth of tree*: 20; *Max features*: sqrt; *Class weight*: balanced, *Feature selection:* RF recursive method. The most significant features were normalised spectra at 475 nm, BNDVI, and normalised spectra at 668 nm, the importance for all selected features are given in Fig. 5 (Appendix C).

Spruce tree health classification

In the spruce tree health classifier model training, the OA was 0.97 for the symptom rule 1 and 0.76, for the symptom rule 2 when evaluated with the validation data. For the independent test data, the OA was 0.96 and 0.83, for the symptom rule 1 and 2, respectively (Table 8). With the symptom rule 1, that used the crown color to classify tree health, the F1-scores were 0.96, 0.40, and 0.98 for the healthy, declined, and dead classes, respectively, for the independent test data (Table 8). For the symptom

Table 5 Results of tree detection in each area with 2021 data, including the reference trees and their detection OA as well as the total number of detected trees

Area	Reference trees			Detected trees
	Field data	Detected	OA	
Viitalampi	305	176	0.58	17,923
Paajasensalo	117	82	0.70	16,361
Murtomäki	112	83	0.74	34,457
Ryhmälehdonmäki	55	50	0.91	11,698

Table 7 Confusion matrix for the species classification model showing predicted and true labels for the independent test dataset Paajasensalo 2019

Predicted label					
		Not-spruce	Spruce	Dead spruce	Tot
True label	Not-spruce	39	13	0	52
	Spruce	0	31	0	31
	Dead spruce	0	0	32	32
	Tot	39	44	32	115

Table 6 Analysis of tree species classification performance

Class	RF validation				RF testing				N-ref (train; val; test)
	Prec	Recall	F1	OA	Prec	Recall	F1	OA	
Not-spruce	0.87	0.75	0.80		1.00	0.75	0.86		153; 60; 52
Spruce	0.75	0.87	0.81		0.70	1.00	0.83		239; 55; 31
Dead spruce	1.00	0.97	0.98		1.00	1.00	1.00		66; 29; 32
OA				0.84				0.89	458; 144; 115

Random Forest (RF) validation statistics were derived from an 80/20 training/validation split, while RF testing results were obtained using the independent Paajasensalo 2019 test dataset. N-ref (train; val; tet): Number of reference trees used for training, validation and testing; OA: Overall Accuracy

Table 8 Analysis of the spruce tree health classification model performance on validation and testing datasets

Symptom rule	Class	RF validation				RF testing				N-ref (train; val; test)
		Prec	Recall	F1-score	OA	Prec	Recall	F1-score	OA	
SR1	Healthy	0.98	0.98	0.98		0.92	1.00	0.96		508; 100; 58
	Declined	1.00	0.33	0.5		1.00	0.25	0.40		11; 3; 4
	Dead	0.95	1.00	0.97		1.00	0.97	0.98		183; 38; 63
	OA				0.97				0.96	702; 141; 125
SR2	Healthy	0.69	0.94	0.80		0.67	0.62	0.64		306; 70; 29
	Declined	0.60	0.09	0.16		0.67	0.73	0.70		215; 33; 33
	Dead	0.95	1.00	0.97		1.00	0.98	0.99		181; 38; 63
	OA				0.76				0.83	702; 141; 125

Random Forest (RF) validation statistics are derived from an 80/20 training/validation split, and RF testing results were obtained using independent test datasets. N-ref (train; val; test): Number of reference trees used for training, validation and testing. SR1: symptom rule 1; SR2: symptom rule 2; OA: Overall accuracy

rule 2 that was evaluating tree health based on both trunk and crown symptoms, the F1-scores were 0.64, 0.70, and 0.99, for the healthy, declined, and dead classes, respectively (Table 8). Confusion matrices for classification on test data are presented in Table 9.

The symptom rule 1 thus gave high classification accuracy for healthy and dead spruce trees. However, this model was poor in detecting declined trees. It is worth noting that with the symptom rule 1 there were only 18 reference trees for the declined class (training: 11, validating: 3, testing: 4) that explains the poor performance of the declined class (Table 8). The symptom rule 2 model gave good detection results for dead spruce trees, but the separation between healthy and declined trees was less accurate (Table 9).

The best performing model for both symptom rules was using all features. The most significant features were the normalised mean spectra at 668 nm, NDVI, and GLI for the symptom rule 1, and the RGBVI, GLI, and normalised mean spectra at 668 nm for the symptom rule 2; importance for all selected features are given in Figs. 6, 7 (Appendix C). For the symptom rule 1, the parameter tuning provided the following main model parameters: *Number of trees:* 200; *Criterion*: gini; *Max depth of tree*: 20; *Maximum features*: sqrt; *Weighting*: balanced. For the symptom rule 2, the parameter tuning gave the following main parameters: *Number of trees*: 300 trees; *Criterion*: entropy; *Maximum depth of tree*: 'None'; *Maximum features*: log2; *Weighting*: no class weight balance.

Detection of fallen trees

The performance of fallen tree detection was evaluated using the field reference trees that had fallen between 2019 and 2021. From the total of 98 fallen reference trees, 24 were excluded from the assessment because they were not detected in the tree detection stage. A total of 62 trees were correctly detected as fallen, 3 fallen trees were undetected, and 9 standing reference trees were detected as fallen. This resulted in a precision of 0.87, a recall of 0.95, and a F1-score of 0.91.

Change analysis in Ruokolahti

The entire monitoring methodology (Fig. 1) was applied to analyse spruce health status and its changes in Ruokolahti area using the datasets from 2019 and 2021. The dataset from 2020 was not included in the analysis because it did not cover the entire study area. After detecting trees (Section "Tree detection") and identifying spruce trees (Section "Tree species classification"), spruce tree health analysis was carried out (Section "Spruce

Table 9 Confusion matrices for spruce tree health classification models with symptom rules 1 and 2 showing predicted and true labels of for the independent test dataset Paajasensalo

Symptom rule 1						Symptom rule 2				
True label	Predicted label					True label	Predicted label			
		Healthy	Declined	Dead	Tot			Healthy	Declined	Dead	Tot
	Healthy	58	0	0	58		Healthy	18	11	0	29
	Declined	3	1	0	4		Declined	9	24	0	33
	Dead	2	0	61	63		Dead	0	1	62	63
	Tot	63	1	61	125		Tot	27	36	62	125

tree health classification"). Fallen trees were detected using the method described in Section "Detection of fallen trees".

The tree health status map in 2021 was generated using the classification results from symptom rule 2 for Ryhmälehdonmäki (Fig. 3a) and Viitalampi (Fig. 3b), representing managed and conserved stands, respectively. The healthy and declined tree classes were merged into a single living tree class because they could not be reliably distinguished. This resulted in two final classes: dead and living. Changes caused by the outbreak are visualised for Ryhmälehdonmäki in Fig. 3c and for Viitalampi in Fig. 3d. In these visualizations, the dead trees show the spatial distribution of the outbreak in 2019. The transition from the living (healthy or declined) tree status in 2019 to the dead tree status in 2021 is represented using a red heatmap, indicating the concentration of new dead trees per hectare in 2021. These hotspot areas emphasise the stands where the outbreak was spreading during the monitoring period. Additionally, the trees that were standing in 2019 (living or dead spruce trees) and had fallen/removed in 2021 are visualised.

In the managed forest, the dead trees appeared as scattered individual trees across the entire forest area, while the fallen/removed trees formed clusters in stands where there were initially no dead trees (Fig. 3c). In the conserved forest, the situation was reversed, with dead trees appearing as clusters, and fallen/removed trees appearing as scattered individual trees often located close to trees that were dead at the beginning of the monitoring (Fig. 3d). Quantitative analysis revealed a significantly larger number of dead trees in the conserved forests (11–12 per hectare) compared to the managed forests (2–3 per hectare) (Table 10). It is interesting to note that in the conserved forests, a large proportion of the detected fallen/removed trees were dead at the beginning of monitoring (45–63%), while in the managed forests, a much smaller proportion of the fallen/removed trees were dead at the beginning of monitoring (6–24%) (Table 10).

Discussion

Remote sensing methodology

This study presented a novel individual tree-based analysis pipeline to monitor bark beetle outbreaks using a low cost UAS multispectral imaging system. The assessment, conducted across a 215 hectares area in Ruokolahti, Southeast Finland, demonstrated good accuracy and yielded consistent analysis outcomes. Despite these promising results, some challenges also emerged. The following discussion addresses these aspects and anticipates advancements and new possibilities as technology continues to progress.

Tree detection and forest structural change analysis relied on the analysis of point clouds generated through the SfM technique. The point clouds were generally dense, with hundreds of points per square meter making them suitable for individual tree-based analysis. Forest density significantly influences the detection of ground points in photogrammetric methods. Therefore, a LiDAR-based DTM was used to provide the ground elevation data and generate CHMs. The performance of tree detection depended on the type of forest management practice; the OA ranged from 0.74 to 0.91 for managed forests and from 0.58 to 0.70 for conserved forest. This dependency on forest management type was attributed to higher tree density and larger proportion of suppressed trees in conserved forests, posing challenges in detecting all trees. Notably, the filtering of reference trees was based solely on height, potentially leading to some reference being obscured by dominant trees and consequently, going undetected. Additionally, the chosen radius of 1 m for tree detection evaluation might have influenced the results. This is because the detected treetop could be positioned differently in the point cloud compared to the initial image-based tree top detection, particularly for large reference trees. Because of these factors, the performance results obtained could potentially be pessimistic. Overall, these results can be considered acceptable for the application, aligning with our earlier findings using the same algorithms (Nevalainen et al. 2017) and contributing to consistent conclusions regarding the outbreak behavior. With a similar tree detection approach using photogrammetric data, Fujimoto et al. (2019) achieved tree detection accuracy of 0.92, but with a sparse forest. Recent UAS-based LiDAR studies have achieved tree detection accuracies ranging from 0.79–0.95 (Sun et al. 2022; Qin et al. 2022).

The detection of missing tree crowns through SfM point cloud comparison yielded a F1-score of 0.91. The good results are consistent with earlier studies (Dandois and Ellis 2013; Guerra-Hernández et al. 2017; Araujo et al. 2021). The efficacy in identifying fallen/removed trees was influenced by the quality of tree detection and point clouds. Specifically, deficient dynamic range in shadowed forest gaps disturbed detection of missing trees locally in some areas. While implementing this method for a multi-year forest inventory is relatively straightforward, it requires some user interaction for setting the method parameters, understanding dataset characteristics, and knowledge of forest management practices in the study stands and adjacent areas. In future studies, it will also be relevant to incorporate methods for detection of trunks laying on the ground. Image-based analysis methods, as demonstrated by Panagiotidis et al. (2019), Thiel et al. (2020), and Polewski et al. (2021), offer a straightforward approach using the proposed multispectral remote sensing approach. Alternatively, LiDAR-based methods, as explored by Heinaro et al. (2023) and Polewski et al. (2015), could also be considered.

In the tree species classification, dead spruce trees were the easiest to classify correctly, while distinguishing between living spruce trees and not-spruce trees showed poorer performance. The resulting 89% OA aligns with previous studies (Nevalainen et al. 2017; Abdollahnejad and Panagiotidis 2020; Deur et al. 2020; Kuzmin et al. 2021). The primary challenge in this stage was the limited number of training samples for not-spruce trees

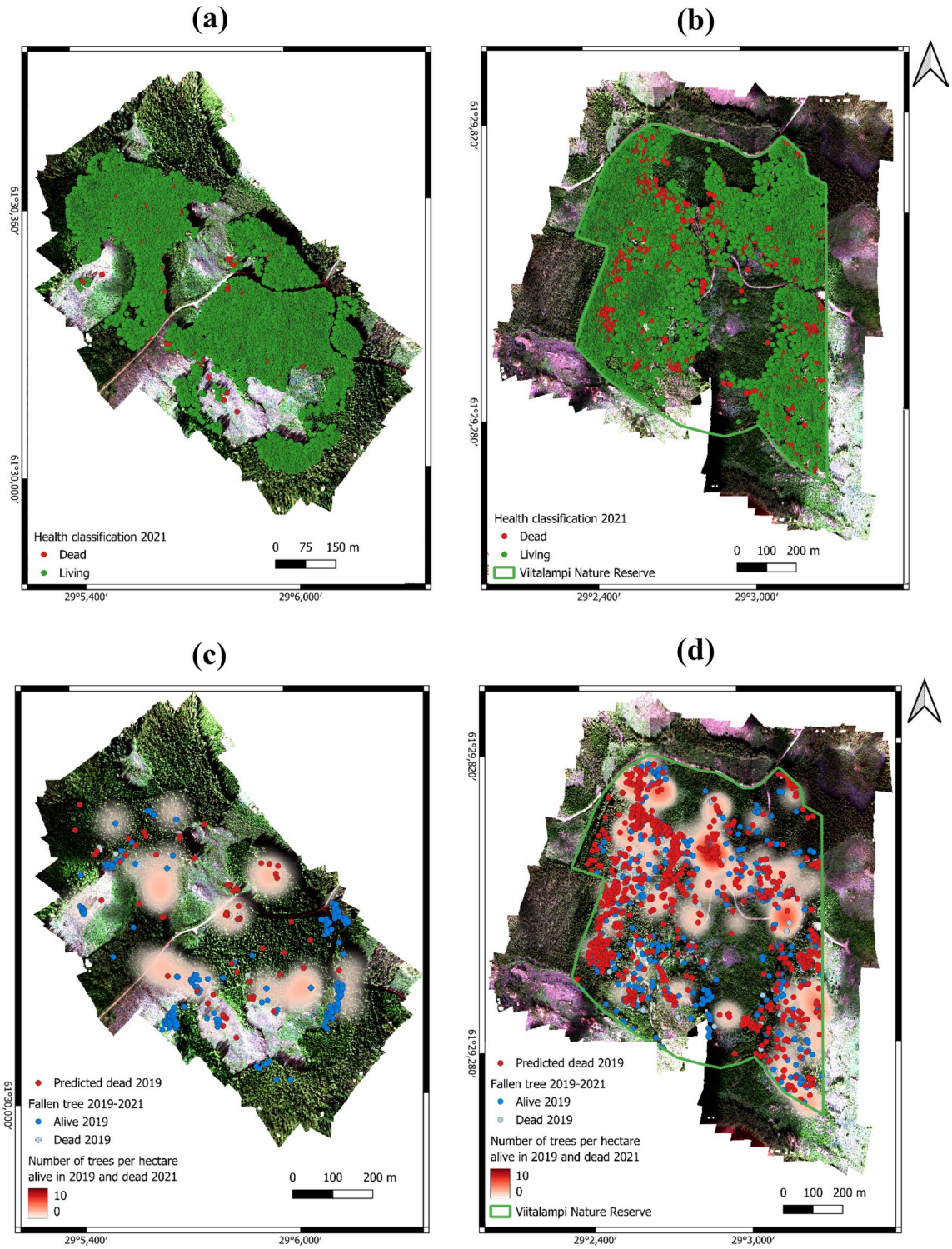

Fig. 3 Spruce health classification to living and dead trees in year 2021 in (**a**) Ryhmälehdonmäki and (**b**) Viitalampi. (**c**) Detected change between years 2019–2021 in Ryhmälehdonmäki and (**d**) Viitalampi. In change analysis, red points indicate spruces that were classified as dead in 2019. Blue points visualise fallen trees that were alive (dark blue) or dead (light blue) in 2019. The heatmap visualises the number of trees per hectare that altered from living 2019 to dead 2021 indicating possible new bark beetle outbreak clusters

because the areas were dominated by spruce trees. It is anticipated that the performance will improve with a larger volume of training data.

In the context of spruce tree health status classification, the best results were obtained for dead trees, while the separation

Table 10 Number of trees for living and dead classes given as an absolute number for the area (No/area) as well as number of trees per hectare (No/ha)

Area	Health class	2019		2021	
		No/area	No/ha	No/area	No/ha
Viitalampi Conserved Area: 76 ha	Living	10,081	133	10,106	133
	Dead	862	11	837	11
	Fallen/removed (living in 2019)	–	–	344	5
	Fallen/removed (dead in 2019)	–	–	285	4
Paajasensalo conserved Area: 39 ha	Living	8472	217	8442	217
	Dead	445	11	475	12
	Fallen/removed (living in 2019)	–	–	60	2
	Fallen/removed (dead in 2019)	–	–	103	3
Ryhmälehdonmäki managed Area: 37 ha	Living	7843	212	7834	212
	Dead	64	2	73	2
	Fallen/removed (living in 2019)	–	–	220	6
	Fallen/removed (dead in 2019)	–	–	13	(0.4)
Murtomäki managed Area: 63 ha	Living	13,450	213	13,493	198
	Dead	181	3	138	2
	Fallen/removed (living in 2019)	–	–	65	1
	Fallen/removed (dead in 2019)	–	–	20	(0.3)

The numbers of fallen/removed trees are given considering whether they were living or dead in 2019

between healthy and declined trees showed poorer accuracy. Symptom rules based on crown color as well as on a combination of trunk and crown color symptoms were compared, in a similar way as in the study by Kanerva et al. (2022). Both symptom rules provided good results in detecting dead trees (F1-score 0.97–0.99). The method based on crown color symptoms (symptom rule 1) provided a high F1-score of 0.96 for classifying green trees, but the training sample of discolored trees was too small for training a reliable classification model. Considering symptom rule 2, a significant portion of trees with green crown exhibited trunk symptoms, leading to their assignment to the declined class. F1-scores of 0.64, 0.70, and 0.99 were obtained at best for the healthy, declined, and dead classes, respectively. The results thus indicated that the spruce trees with green crown but with trunk symptoms could not be distinguished accurately from the healthy spruce trees. On the other hand, these results outperformed the F1-scores of 0.50, 0.52 and 0.81, obtained using RGB images and You-Only-Look-Once deep learning framework by Kanerva et al. (2022) in a similar setting. The enhanced performance is likely attributed to the use of a multispectral camera instead of an RGB camera, consistent with the findings of Turkulainen et al. (2023). The best separation between the healthy and declined classes would be expected in cases where the crowns exhibit changes in color, as observed in the previous study by Junttila et al. (2022); a promising separation of healthy and declined trees was achieved by using multispectral camera and RF-method in a different study area where there were more yellowish/yellow trees in the declined class. In the best scenario, the classification accuracies (recall) were 0.95, 0.46 and 0.96, for the healthy, declined, and dead classes, respectively, in spring, and 0.71, 0.79, 0.99, respectively, in fall season. The obvious improvement of the method should focus on separation of color casts e.g., a transition within green, because typically needle color remains greenish or pale green far late, when bark already has a high damage level due to intensive colonization of *I. typographus*. The trunk symptoms show more intense much earlier than crown symptoms. The status of infestation will impact on the detection rate of infested trees, as highlighted in previous studies by Klouček et al., (2019), Junttila et al., (2022), and Huo et al., (2023). Increasing the volume of training data, coupled with advancements in camera and analysis technology, is expected to enhance the classification accuracy for separating the healthy and declined trees.

In 2019–2020, this study used the previous generation of UAS equipment, lacking precise RTK GNSS positioning, whereas the 2021 dataset was collected using a new generation of UAS equipment equipped with RTK GNSS. Anticipated advancements include overcoming many of the identified challenges with the improved UAS remote sensing equipment, leveraging RTK GNSS for precise positioning, and enhancing camera technologies. Radiometric challenges arising from changing illumination conditions during flights are also expected to see improvements with advancements in incident light sensors and processing (e.g., Suomalainen et al. 2021).

In this study, multispectral cameras were used, facilitating the creation of an inexpensive and lightweight UAS monitoring system. The use of single-sensor solutions provided all necessary datasets for monitoring. However, employing more advanced remote sensing instruments could potentially enhance performance levels. Improved spectral resolution achieved through hyperspectral imaging, in particular, might offer benefits, especially for early detection of bark beetle damage and

species classification (Lin et al. 2023; Turkulainen et al. 2023). Also, thermal imaging could support analysis of tree health status (Zakrzewska et al. 2023; Junttila et al. 2017). LiDAR point clouds could provide advantages in the individual tree detection (Kaartinen et al. 2012; Jaskierniak et al. 2021) and canopy gap and structure analysis (Chung et al. 2022), which could improve performance of fallen tree detection. The drawbacks of these systems would include elevated costs, increased system weights, and added complexity. Nevertheless, the remote sensing technology proposed in this study was proven to be highly relevant, demonstrating valuable performance for monitoring tasks. It is worth noting that the performance levels of these low-cost sensing systems are also improving, and many of the identified challenges could be successfully addressed.

ML techniques are also evolving rapidly and recent advancements in deep learning methods have demonstrated enhanced accuracies (Nezami et al. 2020; Minarik et al. 2021; Onishi & Ise 2021; Safonova et al. 2022; Turkulainen et al. 2023). However, deep learning requires large training datasets, which are often challenging to obtain. This challenge was also faced in this study, and therefore classical ML techniques were successfully used. For tasks focused on detecting living and dead trees, the state-of-the-art object detection networks and low-cost RGB camera-based approaches could already provide acceptable results, as shown in recent studies (e.g., Kanerva et al. 2022; Safonova et al. 2022). On the other hand, for more challenging tasks, such as declined tree detection and "green attack" detection, the multispectral and hyperspectral camera system have shown promising results (Huo et al. 2023; Turkulainen et al. 2023).

Insights into changes in bark beetle outbreak monitoring sites

The principal contribution of this study was the development of a comprehensive UAS multispectral imaging pipeline for monitoring changes in the forest ecosystem due to bark beetle outbreak. Utilising this new pipeline, maps and statistics illustrating changes in the study areas were generated, providing insights into the impacts and changes within different forest environments (Fig. 3; Table 10). To the best of the authors' knowledge, this study was the first to present a comprehensive UAS-based multiyear monitoring approach for an area affected by a bark beetle outbreak.

This study used the change of the spruce tree status from healthy to declined, dead or fallen/removed during the period as the indicators of the spread and host colonization of the bark beetle outbreak (Fig. 3). Detection of dead trees can be efficiently performed using remote sensing images, as discussed previously, making it a promising approach for monitoring the outbreak. However, it should be noted that the results indicated that in the conserved forest, 40–60% of fallen, and in the managed forest, 77–94% of fallen/removed trees were alive at the beginning of the monitoring period (Table 10. In the studied areas, the analysis of standing dead trees alone would not have provided comprehensive information about changes in the forest. Therefore, it was relevant to estimate the number of fallen/removed trees when drawing conclusions about the impact of the outbreak. On the other hand, our study did not extend to the identification of the actual fallen tree trunks. Especially in managed areas, part of the fallen (or removed) trees can be explained as clear cuttings or thinning, but in the conserved areas the majority of fallen trees were killed by the bark beetle four to seven years before falling due to abundance of optimal resources available for the pest (Mezei et al. 2014).

The overall analysis showed great differences in the conserved and managed areas on the numbers of dead trees per hectare as well as the rate of new tree deaths (Fig. 3; Table 10). The observations on mortality patterns in Section "Change analysis in Ruokolahti" are consistent with expected forest management operations and their impacts in conserved and managed forests. In the managed forests, sanitary cuttings had taken place to remove stands with the dead and infested trees, and these cuttings are likely to explain the clusters of fallen/removed trees in the area. As a result of an outbreak management, the numbers of newly died trees were low, and only 2–3 dead trees per hectare appeared. Meanwhile, in the conserved forest, the outbreak was spreading in an uncontrolled way, which appeared as large numbers of detected dead trees (11–12 per hectare) and great mortality rates (Fig. 3, Table 10), as also Kärvemo et al. (2017) observed in other study areas. According to Eriksson et al. (2007), higher volume and basal area of spruce elevate a risk of a bark beetle disturbance, which was evident in the conserved forests. The scattered fallen/removed trees indicated a pattern of host searching and colonization by the beetle (Wermelinger 2004). The fact that only a few fallen/removed trees were dead in the beginning of monitoring in the managed forest also indicated an influence of sanitary cuttings and an active removal of infested trees, while in the conserved forests the trees were dying and then falling. It can be concluded that the observed impacts indicate successful control of infestation in the managed forests. On the other hand, the situation in the conserved forests shows that if the outbreak is not controlled, the damage can be dramatic, supporting the findings by Kärvemo et al. (2017) on forest conservation measures, creating a high risk of coming *I. typographus* infestations.

While the detection of dead trees yielded good results, challenges arose in classifying declined trees. These challenges were attributed to the small portion of trees with crown color symptoms in the area and the difficulty in identifying trees with trunk

symptoms among the set of spruce trees with a green crown. In particular, finding declined trees at early stages is crucial when the goal is to actively mitigate the spread of bark beetles. The emerging remote sensing technologies also offer many possibilities in this regard, as envisioned in Section "Remote sensing methodology"

In comparison to visual field surveys, the UAS method offers a more complete insight on how the infestation has progressed in the entire area. This information could be used, for example, by risk modelers, forest experts, and forest managers to understand the dynamics of the infestation. Also, private and public forest owners and state organizations could use this information as documentation of the destruction due to outbreak e.g., to make management decisions or for insurance purposes. The analysis results clearly showed the benefits of active control measures in managed forests, in comparison to the uncontrolled spread of the outbreak in the conserved forests.

On the other hand, the aerial surveys by UAS did not completely replace field surveys when considering different aspects of outbreak monitoring. The field surveys collect versatile information about the infestation, particularly the severity of the trunk symptoms such as intensity of entrance and exit holes in the bark or new resin flows (Blomqvist et al. 2018; Table 2). The first symptoms such as new entrance holes can only be observed in close range to the trunk. Our results on finding declined trees with visible trunk symptoms and still green crown using the multispectral aerial images indicated promises in comparison to the earlier study using RGB images by Kanerva et al. (2022); our F1-scores in the study area were 0.64, 0.70, and 0.99 in comparison to 0.49, 0.52 and 0.81 of Kanerva et al. (2022). Our further studies will focus on improving the remote sensing component by using advancing multispectral and hyperspectral sensors and high temporal resolution datasets to enable more sensitive detection of tree decline using remote sensing techniques instead of field inspection, e.g., following the approach by Huo et al. (2023). Also, our objective is to implement fast decision support tools for forest managers during the outbreak.

The results strongly suggest that a UAS-based approach is an efficient and precise tool for monitoring a bark beetle outbreak area. The proposed method demonstrated high accuracy in quantifying the impacts of various management strategies, such as sanitation and salvage cuttings. The methodology could be further employed in various tasks related to outbreak management, including the consideration of impacts of mixed stands with a larger share of deciduous tree species (Müller et al. 2022). In future analyses, UAS techniques could be leveraged to characterise forest regeneration and to inform restoration programs (Nuijten et al. 2021).

Conclusion

This study developed and evaluated a novel analysis pipeline for monitoring the European spruce bark beetle outbreak areas on an individual tree basis, using multitemporal data collected by a low-cost multispectral UAS remote sensing system. The methodology was then employed to gain insights into changes at a multiyear bark beetle monitoring site in southeastern Finland, comprising two conserved and two managed forest areas. The approach included tree detection, tree species classification, spruce tree health classification, and change analysis including fallen/removed tree detection and mortality hotspot evaluation. The performance was assessed using unseen test datasets. Individual trees were detected by analyzing photogrammetric point clouds with an overall accuracy (OA) of 0.58–0.91, depending on the complexity of the forest area. Species classification using random forest algorithm presented an OA of 0.89. For health status estimation, the study compared the use of the crown color symptoms alone as well as an integrated symptom scoring using both trunk and crown symptoms, achieving OAs ranging between 0.83 and 0.96. In the spruce tree health estimation, the healthy and dead spruce trees were detected with a high accuracy, whereas identification of intermediate states between healthy and dead was less accurate. The study further showed that fallen/removed trees could be detected using multi-temporal structure-from-motion point clouds with a F1-score of 0.91. The maps depicting dead and fallen/removed spruce trees, along with newly attacked stands demonstrated the evolution of the outbreak between August 2019 and August 2021. Results indicated successful control of the outbreak in terms of tree mortality in managed stands while the outbreak resulted in disastrous tree mortality in conserved stands. The produced monitoring information could serve various stakeholders by illustrating and documenting the impact of the outbreak on the forest area. Additionally, it creates timely risk assessment and management measures to control the bark beetle outbreak.

Appendix A

See Fig. 4.

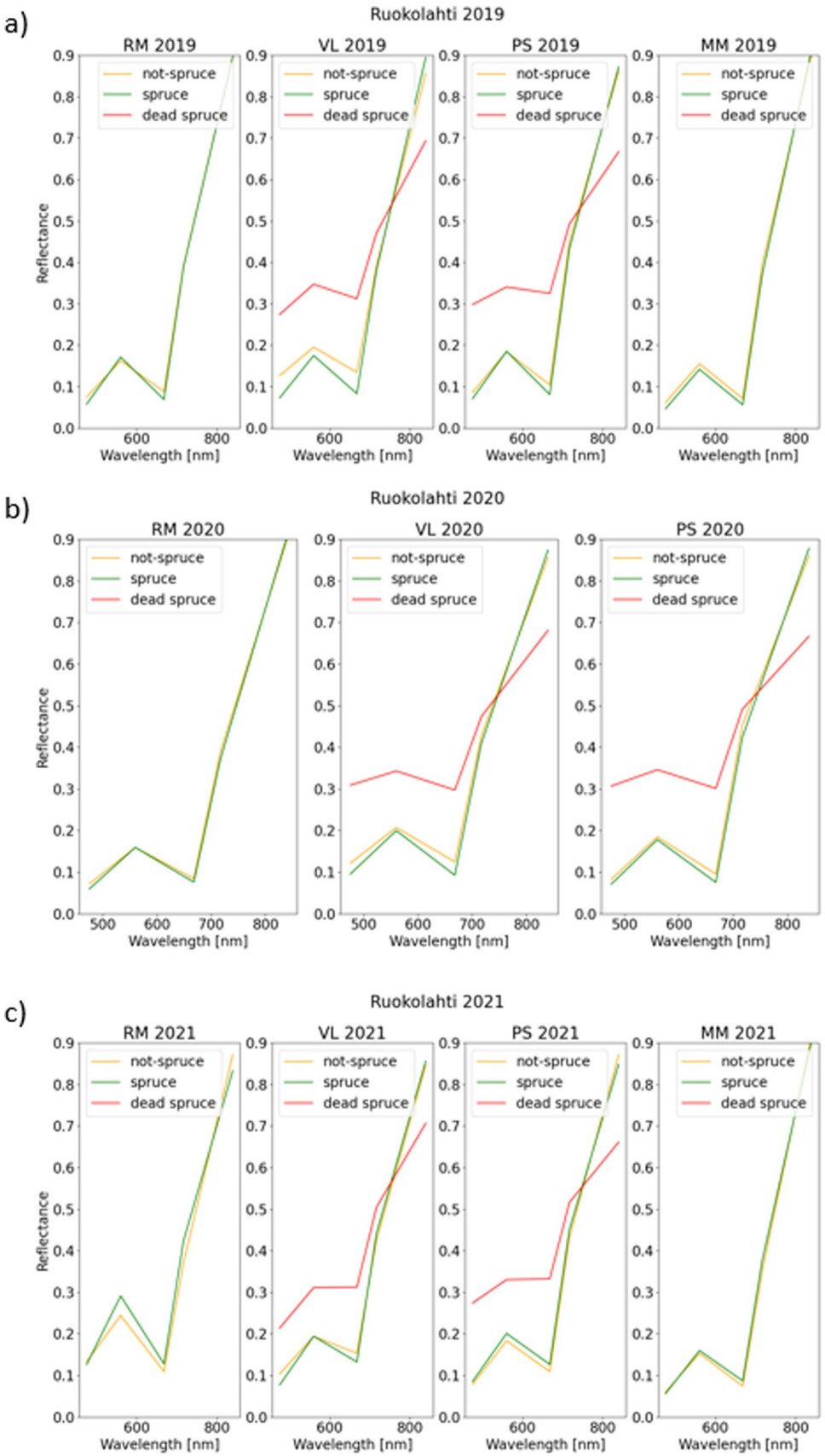

Fig. 4 Normalised mean reflectance spectra for the three classes of species reference trees in Ruokolahti (**a**) 2019, (**b**) 2020 and (**c**) 2021. Orange: not-spruce, green: spruce, red: dead spruce. In Ryhmälehdonmäki and Murtomäki, there were no dead spruces in the collected reference dataset

Appendix B

See Table 11.

Table 11 Equations of extracted VIs

Feature	Equation	Reference
Normalised spectral value	$\text{Reflectance}_B / \sqrt{\sum \text{Reflectance}_B^{\,2}}$ (B ∈ 1…number of bands)	
ARVI	$\frac{R_{800}-(R_{670}-1*(R_{470}-R_{670}))}{R_{800}+(R_{670}-1*(R_{470}-R_{670}))}$	Kaufman and Tanré (1992)
ARVI2	$-0.18 + (1.17\frac{R_{800}-R_{670}}{R_{800}+R_{670}})$	Kaufman and Tanré (1992)
BNDVI	$\frac{R_{800}-R_{440}}{R_{800}+R_{550}}$	Yang et al. (2004)
CI	$\frac{R_{670}-R_{445}}{R_{670}}$	Escadafal et al. (1994)
CIG	$\frac{R_{800}}{R_{670}} - 1$	Gitelson et al. (2003)
CVI	$R_{800}\frac{R_{670}}{R_{550}^{\,2}}$	Vincini et al. (2008)
DATT1	$\frac{R_{850}-R_{710}}{R_{850}-R_{680}}$	Datt (1999)
DATT 6	$\frac{R_{860}}{R_{550}*R_{708}}$	Datt (1998)
ExG	$2 * R_{550} - R_{670} - R_{470}$	Woebbecke et al. (1995)
ExGR	$2 * R_{550} - R_{670} - R_{470} - 1.4 * R_{670} - R_{470}$	Neto (2004)
ExR	$1.4 * R_{670} - R_{470}$	Meyer and Neto (2008)
GLI	$\frac{2*R_{550}-R_{670}-R_{475}}{2*R_{550}+R_{670}+R_{475}}$	Gobron et al. (2000)
GNDVI	$\frac{R_{800}-R_{550}}{R_{800}+R_{550}}$	Gitelson et al. (1996)
LogR	$log\frac{R_{800}}{R_{670}}$	
MTVI	$1.2(1.2(R_{800} - R_{550}) - 2.5(R_{670} - R_{550}))$	Haboudane (2004)
NDRE	$\frac{R_{790}-R_{720}}{R_{790}+R_{720}}$	Barnes et al. (2000)
NDVI	$\frac{R_{800}-R_{670}}{R_{800}+R_{670}}$	Tucker (1979)
OSAVI	$(1+0.16)\frac{R_{800}-R_{670}}{R_{800}+R_{670}+0.16}$	Wu et al. (2008)
RDVI	$\frac{R_{800}-R_{670}}{\sqrt{R_{800}+R_{670}}}$	Haboudane (2004)
RE1	$\frac{R_{850}-R_{710}}{R_{850}/R_{680}}$	
RGBVI	$\frac{R_{550}^{\,2}-R_{470}*R_{670}}{R_{550}^{\,2}+R_{470}*R_{670}}$	Bendig et al. (2015)
RGBVI2	$\frac{R_{550}^{\,2}-R_{470}*R_{670}}{R_{550}^{\,2}} + R_{470} * R_{670}$	
SAVI	$(1+0.5)\frac{R_{800}-R_{670}}{R_{800}+R_{670}+0.5}$	Huete (1988)
TCI	$\frac{(R_{800}+1.5*R_{550})-R_{675}}{R_{800}-R_{700}}$	Gao (2006)

Appendix C

See Figs. 5, 6, 7.

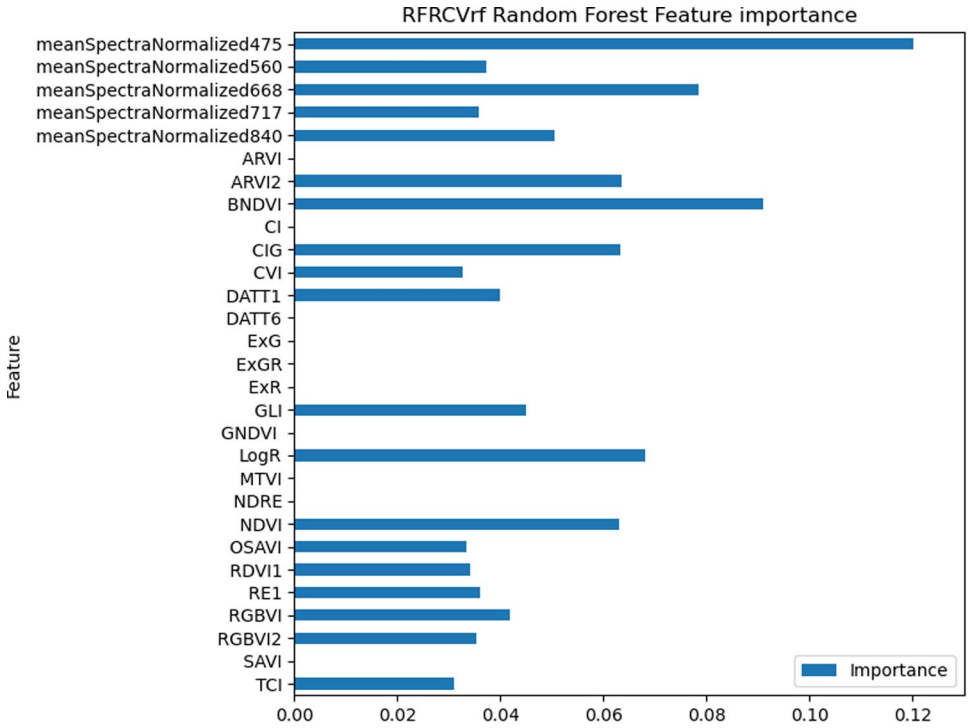

Fig. 5 Random forest feature importance for species classification

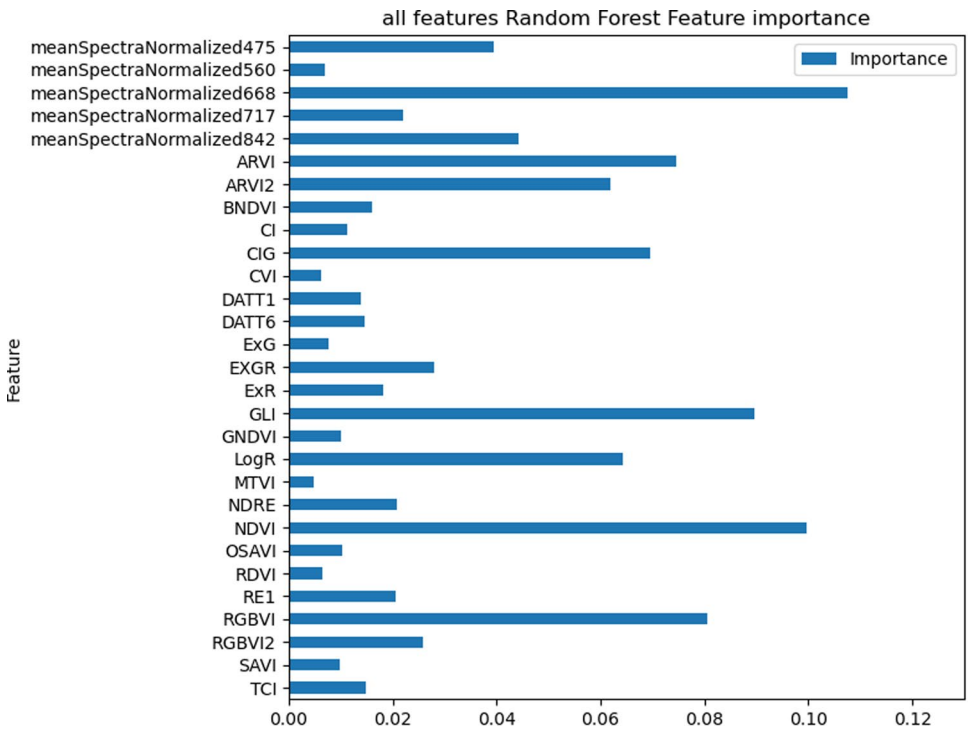

Fig. 6 Random forest feature importance for health estimation, symptom rule 1

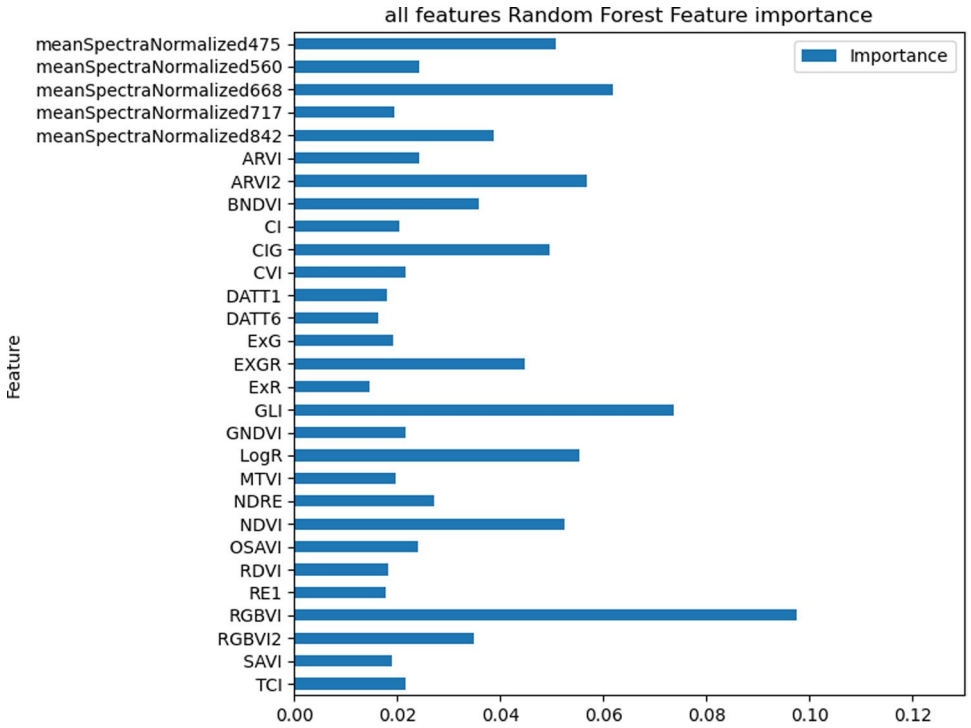

Fig. 7 Random forest feature importance for health estimation, symptom rule 2

Acknowledgements We wish to thank Aleksi Flyktman, Micke Malm and Juho Äyräs for the help with the fieldwork. Tornator Ltd., particularly the former head of forest resources Maarit Sallinen and the forest data manager Kimmo Kortelainen are thanked for enabling the study in Ruokolahti. We also thank Stora Enso Ltd. for facilities in Viitalampi during the annual field work.

Author contributions Conceptualization: E.H, P.L.-S.; Data curation: M.Ö., R.A.O, R.N., N.K., M.P.-A., J.T.; Investigation: M.Ö.; Methodology: M.Ö., E.H., R.A.O., R.N.; Resources: E.H., R.A.O., R.N., T.H., N.K., M.P.-A., J.T., P.L.-S.; Software: R.A.O., R.N., O.N.; Writing – original draft: M.Ö., E.H; Writing – review & editing: M.Ö., E.H., R.A.O., R.N., T.H., N.K., M.P.-A., J.T., O.N., P.L.-S.; Visualization: M.Ö., E.H.; Supervision: E.H., R.N., P.L.-S.; Project administration: E.H., P.L.-S.; Funding acquisition: E.H., P.L.-S.

Funding Open Access funding provided by National Land Survey of Finland. This research was funded by the Academy of Finland under grants 357380, 353263, 353264, by the Ministry of Agriculture and Forestry of Finland with the projects MONITUHO (no. 647/03.02.06.00/2018), SPRUCERISK (no. VN/5292/2021), and MMM_UNITE (no. VN/3482/2021), and by the Marjatta and Eino Kolli Foundation with IPSRISK project (no. 1103). This study was affiliated to the Academy of Finland Flagship Forest–Human–Machine Interplay—Building Resilience, Redefining Value Networks and Enabling Meaningful Experiences (UNITE) (decision no. 337127) and the Atmosphere and Climate Competence Center (ACCC) (decision no. 337552).

Data availability The authors do not have permission to share data.

Code availability Not applicable.

Declarations

Conflicts of interest The authors declare no competing interests.

Open Access This article is licensed under a Creative Commons Attribution 4.0 International License, which permits use, sharing, adaptation, distribution and reproduction in any medium or format, as long as you give appropriate credit to the original author(s) and the source, provide a link to the Creative Commons licence, and indicate if changes were made. The images or other third party material in this article are included in the article's Creative Commons licence, unless indicated otherwise in a credit line to the material. If material is not included in the article's Creative Commons licence and your intended use is not permitted by statutory regulation or exceeds the permitted use, you will need to obtain permission directly from the copyright holder. To view a copy of this licence, visit http://creativecommons.org/licenses/by/4.0/.

References

Abdollahnejad A, Panagiotidis D (2020) Tree species classification and health status assessment for a mixed broadleaf-conifer forest with UAS multispectral imaging. Remote Sens 12:3722. https://doi.org/10.3390/rs12223722

Araujo RF, Grubinger S, Celes CHS, Negrón-Juárez RI, Garcia M, Dandois JP, Muller-Landau HC (2021) Strong temporal variation in treefall and branchfall rates in a tropical forest is related to extreme rainfall: results from 5 years of monthly drone data for a 50 ha plot. Biogeosciences 18:6517–6531. https://doi.org/10.5194/bg-18-6517-2021

Barnes EM, Clarke TR, Richards SE, Colaizzi PD, Haberland J, Kostrzewski M, Waller P, Choi C, Riley E, Thompson T, Lascano RJ, Li H, Moran MS (2000) Coincident detection of crop water stress, nitrogen status, and canopy density using ground-based

multispectral data. In: 5th international conference on precision agriculture, Bloomington, 16–19 July 2000, 1–15
Barrere J, Reineking B, Cordonnier T, Kulha N, Honkaniemi J, Peltoniemi M, Korhonen KT, Ruiz-Benito P, Zavala MA, Kunstler G (2023) Functional traits and climate drive interspecific differences in disturbance-induced tree mortality. Glob Change Biol 29:2836–2851. https://doi.org/10.1111/gcb.16630
Bárta V, Hanuš J, Dobrovolný L, Homolová L (2022) Comparison of field survey and remote sensing techniques for detection of bark beetle-infested trees. For Ecol Manage 506:119984. https://doi.org/10.1016/j.foreco.2021.119984
Bendig J, Yu K, Aasen H, Bolten A, Bennertz S, Broscheit J, Gnyp ML, Bareth G (2015) Combining UAV-based plant height from crop surface models, visible, and near infrared vegetation indices for biomass monitoring in barley. Int J Appl Earth Obs Geoinf 39:79–87. https://doi.org/10.1016/j.jag.2015.02.012
Bergstra J, Bengio Y (2012) Random search for hyper-parameter optimization. J Mach Learn Res 13:281–305
Blomqvist M, Kosunen M, Starr M, Kantola T, Holopainen M, Lyytikäinen-Saarenmaa P (2018) Modelling the predisposition of Norway spruce to *Ips typographus* L. infestation by means of environmental factors in southern Finland. Eur J Forest Res 137:675–691. https://doi.org/10.1007/s10342-018-1133-0
Breiman L (2001) Random forests. Mach Learn 45:5–32. https://doi.org/10.1023/A:1010933404324
Chung C-H, Wang J, Deng S-L, Huang C (2022) Analysis of canopy gaps of coastal broadleaf forest plantations in Northeast Taiwan Using UAV lidar and the weibull distribution. Remote Sensing 14:667. https://doi.org/10.3390/rs14030667
D'Odorico P, Schönbeck L, Vitali V, Meusburger K, Schaub M, Ginzler C, Zweifel R, Velasco VME, Gisler J, Gessler A, Ensminger I (2021) Drone-based physiological index reveals long-term acclimation and drought stress responses in trees. Plant Cell Environ 44:3552–3570. https://doi.org/10.1111/pce.14177
Dandois JP, Ellis EC (2013) High spatial resolution three-dimensional mapping of vegetation spectral dynamics using computer vision. Remote Sens Environ 136:259–276. https://doi.org/10.1016/j.rse.2013.04.005
Dash JP, Watt MS, Pearse GD, Heaphy M, Dungey HS (2017) Assessing very high resolution UAV imagery for monitoring forest health during a simulated disease outbreak. ISPRS J Photogramm Remote Sens 131:1–14. https://doi.org/10.1016/j.isprsjprs.2017.07.007
Datt B (1998) Remote sensing of chlorophyll a, chlorophyll b, chlorophyll a+b, and total carotenoid content in eucalyptus leaves. Remote Sens Environ 66:111–121. https://doi.org/10.1016/S0034-4257(98)00046-7
Datt B (1999) A new reflectance index for remote sensing of chlorophyll content in higher plants: tests using eucalyptus leaves. J Plant Physiol 154:30–36. https://doi.org/10.1016/S0176-1617(99)80314-9
Deur M, Gašparović M, Balenović I (2020) Tree species classification in mixed deciduous forests using very high spatial resolution satellite imagery and machine learning methods. Remote Sens 12:3926. https://doi.org/10.3390/rs12233926
Ecke S, Dempewolf J, Frey J, Schwaller A, Endres E, Klemmt H-J, Tiede D, Seifert T (2022) UAV-based forest health monitoring: a systematic review. Remote Sens 14:3205. https://doi.org/10.3390/rs14133205
Eriksson M, Neuvonen S, Roininen H (2007) Retention of wind-felled trees and the risk of consequential tree mortality by the European spruce bark beetle *Ips typographus* in Finland. Scand J for Res 22:516–523. https://doi.org/10.1080/02827580701800466
Escadafal R, Belghit A, Ben-Moussa A (1994) Indices spectraux pour la télédétection de la dégradation des milieux naturels en Tunisie aride. In: Guyot, G. réd., Actes du 6eme Symposium international sur les mesures physiques et signatures en télédétection, Val d'Isère (France), pp 253–259
Fraser BT, Congalton RG (2021) Monitoring fine-scale forest health using unmanned aerial systems (UAS) multispectral models. Remote Sens 13:4873. https://doi.org/10.3390/rs13234873
Fujimoto A, Haga C, Matsui T, Machimura T, Hayashi K, Sugita S, Takagi H (2019) An end to end process development for UAV-SfM based forest monitoring: individual tree detection, species classification and carbon dynamics simulation. Forests 10:680. https://doi.org/10.3390/f10080680
Gao J (2006) Canopy chlorophyll estimation with hyperspectral remote sensing. Dissertation, Kansas State University, Department of Geography, Manhattan, Kansas. http://hdl.handle.net/2097/252
Gitelson AA, Kaufman YJ, Merzlyak MN (1996) Use of a green channel in remote sensing of global vegetation from EOS-MODIS. Remote Sens Environ 58:289–298. https://doi.org/10.1016/S0034-4257(96)00072-7
Gitelson AA, Viña A, Arkebauer TJ, Rundquist DC, Keydan G, Leavitt B (2003) Remote estimation of leaf area index and green leaf biomass in maize canopies. Geophys Res Lett 30:2002GL016450. https://doi.org/10.1029/2002GL016450
Gobron N, Pinty B, Verstraete MM, Widlowski J-L (2000) Advanced vegetation indices optimized for up-coming sensors: design performance and applications. IEEE Trans Geosci Remote Sens 38(6):2489–2505. https://doi.org/10.1109/36.885197
Grybas H, Congalton RG (2021) A Comparison of multi-temporal RGB and multispectral UAS imagery for tree species classification in heterogeneous new hampshire forests. Remote Sens 13:2631. https://doi.org/10.3390/rs13132631
Guerra-Hernández J, González-Ferreiro E, Monleón V, Faias S, Tomé M, Díaz-Varela R (2017) Use of multi-temporal UAV-derived imagery for estimating individual tree growth in pinus pinea stands. Forests 8:300. https://doi.org/10.3390/f8080300
Haboudane D (2004) Hyperspectral vegetation indices and novel algorithms for predicting green LAI of crop canopies: modeling and validation in the context of precision agriculture. Remote Sens Environ 90:337–352. https://doi.org/10.1016/j.rse.2003.12.013
Hartling S, Sagan V, Maimaitijiang M (2021) Urban tree species classification using UAV-based multi-sensor data fusion and machine learning. Gisci Remote Sens 58:1250–1275. https://doi.org/10.1080/15481603.2021.1974275
Heinaro E, Tanhuanpää T, Vastaranta M, Yrttimaa T, Kukko A, Hakala T, Mattsson T, Holopainen M (2023) Evaluating factors impacting fallen tree detection from airborne laser scanning point clouds. Remote Sens 15:382. https://doi.org/10.3390/rs15020382
Hlásny T, König L, Krokene P, Lindner M, Montagné-Huck C, Müller J, Qin H, Raffa KF, Schelhaas M-J, Svoboda M, Viiri H, Seidl R (2021) Bark beetle outbreaks in Europe: state of knowledge and ways forward for management. Curr for Rep 7:138–165. https://doi.org/10.1007/s40725-021-00142-x
Honkavaara E, Näsi R, Oliveira R, Viljanen N, Suomalainen J, Khoramshahi E, Hakala T, Nevalainen O, Markelin L, Vuorinen M, Kankaanhuhta V, Lyytikäinen-Saarenmaa P, Haataja L (2020) Using multitemporal hyper- and multispectral uav imaging for detecting bark beetle infestation on norway spruce. Int Arch Photogramm Remote Sens Spatial Inf Sci XLIII-B3-2020:429–434
Huete AR (1988) A soil-adjusted vegetation index (SAVI). Remote Sens Environ 25:295–309. https://doi.org/10.1016/0034-4257(88)90106-X
Huo L, Lindberg E, Bohlin J, Persson HJ (2023) Assessing the detectability of European spruce bark beetle green attack in multispectral drone images with high spatial- and temporal resolutions. Remote Sens Environ 287:113484. https://doi.org/10.1016/j.rse.2023.113484

Iglhaut J, Cabo C, Puliti S, Piermattei L, O'Connor J, Rosette J (2019) Structure from motion photogrammetry in forestry: a review. Curr for Rep 5:155–168. https://doi.org/10.1007/s40725-019-00094-3

Jaskierniak D, Lucieer A, Kuczera G, Turner D, Lane PNJ, Benyon RG, Haydon S (2021) Individual tree detection and crown delineation from unmanned aircraft system (UAS) LiDAR in structurally complex mixed species eucalypt forests. ISPRS J Photogramm Remote Sens 171:171–187. https://doi.org/10.1016/j.isprsjprs.2020.10.016

Junttila S, Vastaranta M, Hämäläinen J, Latva-käyrä P, Holopainen M, Hernández Clemente R, Hyyppä H, Navarro-Cerrillo RM (2017) Effect of forest structure and health on the relative surface temperature captured by airborne thermal imagery—case study in Norway Spruce-dominated stands in Southern Finland. Scand J for Res 32:154–165. https://doi.org/10.1080/02827581.2016.1207800

Junttila S, Näsi R, Koivumäki N, Imangholiloo M, Saarinen N, Raisio J, Holopainen M, Hyyppä H, Hyyppä J, Lyytikäinen-Saarenmaa P, Vastaranta M, Honkavaara E (2022) Multispectral imagery provides benefits for mapping spruce tree decline due to bark beetle infestation when acquired late in the season. Remote Sens 14:909. https://doi.org/10.3390/rs14040909

Kaartinen H, Hyyppä J, Yu X, Vastaranta M, Hyyppä H, Kukko A, Holopainen M, Heipke C, Hirschmugl M, Morsdorf F, Næsset E, Pitkänen J, Popescu S, Solberg S, Wolf BM, Wu J-C (2012) An International comparison of individual tree detection and extraction using airborne laser scanning. Remote Sens 4:950–974. https://doi.org/10.3390/rs4040950

Kanerva H, Honkavaara E, Näsi R, Hakala T, Junttila S, Karila K, Koivumäki N, Alves Oliveira R, Pelto-Arvo M, Pölönen I, Tuviala J, Östersund M, Lyytikäinen-Saarenmaa P (2022) Estimating tree health decline caused by *Ips typographus* L. from UAS RGB images using a deep one-stage object detection neural network. Remote Sens 14:6257. https://doi.org/10.3390/rs14246257

Kärvemo S, Van Boeckel TP, Gilbert M, Grégoire J-C, Schroeder M (2014) Large-scale risk mapping of an eruptive bark beetle—importance of forest susceptibility and beetle pressure. For Ecol Manag 318:158–166. https://doi.org/10.1016/j.foreco.2014.01.025

Kärvemo S, Björkman C, Johansson T, Weslien J, Hjältén J (2017) Forest restoration as a double-edged sword: the conflict between biodiversity conservation and pest control. J Appl Ecol 54:1658–1668. https://doi.org/10.1111/1365-2664.12905

Kaufman YJ, Tanre D (1992) Atmospherically resistant vegetation index (ARVI) for EOS-MODIS. IEEE Trans Geosci Remote Sens 30:261–270. https://doi.org/10.1109/36.134076

Klouček T, Komárek J, Surový P, Hrach K, Janata P, Vašíček B (2019) The use of UAV mounted sensors for precise detection of bark beetle infestation. Remote Sens 11:1561. https://doi.org/10.3390/rs11131561

Kosunen M, Lyytikäinen-Saarenmaa P, Ojanen P, Blomqvist M, Starr M (2019) Response of soil surface respiration to storm and *Ips typographus* (L.) disturbance in boreal Norway spruce stands. Forests 10(4):307. https://doi.org/10.3390/f10040307

Kuzmin A, Korhonen L, Kivinen S, Hurskainen P, Korpelainen P, Tanhuanpää T, Maltamo M, Vihervaara P, Kumpula T (2021) Detection of european aspen (*Populus tremula* L.) based on an unmanned aerial vehicle approach in boreal forests. Remote Sens 13:1723. https://doi.org/10.3390/rs13091723

Lefsky MA, Cohen WB, Acker SA, Parker GG, Spies TA, Harding D (1999) Lidar remote sensing of the canopy structure and biophysical properties of douglas-fir western hemlock forests. Remote Sens Environ 70:339–361. https://doi.org/10.1016/S0034-4257(99)00052-8

Liang X, Hyyppä J, Kaartinen H, Lehtomäki M, Pyörälä J, Pfeifer N, Holopainen M, Brolly G, Francesco P, Hackenberg J, Huang H, Jo H-W, Katoh M, Liu L, Mokroš M, Morel J, Olofsson K, Poveda-Lopez J, Trochta J, Wang D, Wang J, Xi Z, Yang B, Zheng G, Kankare V, Luoma V, Yu X, Chen L, Vastaranta M, Saarinen N, Wang Y (2018) International benchmarking of terrestrial laser scanning approaches for forest inventories. ISPRS J Photogramm Remote Sens 144:137–179. https://doi.org/10.1016/j.isprsjprs.2018.06.021

Liang X, Kukko A, Balenovic I, Saarinen N, Junttila S, Kankare V, Holopainen M, Mokros M, Surovy P, Kaartinen H, Jurjevic L, Honkavaara E, Nasi R, Liu J, Hollaus M, Tian J, Yu X, Pan J, Cai S, Virtanen J-P, Wang Y, Hyyppa J (2022) Close-range remote sensing of forests: the state of the art, challenges, and opportunities for systems and data acquisitions. IEEE Geosci Remote Sens Mag 10:32–71. https://doi.org/10.1109/MGRS.2022.3168135

Lin Q, Huang H, Wang J, Chen L, Du H, Zhou G (2023) Early detection of pine shoot beetle attack using vertical profile of plant traits through UAV-based hyperspectral, thermal, and lidar data fusion. Int J Appl Earth Obs Geoinf 125:103549. https://doi.org/10.1016/j.jag.2023.103549

Meyer GE, Neto JC (2008) Verification of color vegetation indices for automated crop imaging applications. Comput Electron Agric 63:282–293. https://doi.org/10.1016/j.compag.2008.03.009

Mezei P, Grodzki W, Blaženec M, Škvarenina J, Brandýsová V, Jakuš R (2014) Host and site factors affecting tree mortality caused by the spruce bark beetle (*Ips typographus*) in mountainous conditions. For Ecol Manage 331:196–207. https://doi.org/10.1016/j.foreco.2014.07.031

Michez A, Piégay H, Lisein J, Claessens H, Lejeune P (2016) Classification of riparian forest species and health condition using multi-temporal and hyperspatial imagery from unmanned aerial system. Environ Monit Assess 188:146. https://doi.org/10.1007/s10661-015-4996-2

Minařík R, Langhammer J, Lendzioch T (2021) Detection of bark beetle disturbance at tree level using UAS multispectral imagery and deep learning. Remote Sens 13:4768. https://doi.org/10.3390/rs13234768

Müller M, Olsson P-O, Eklundh L, Jamali S, Ardö J (2022) Features predisposing forest to bark beetle outbreaks and their dynamics during drought. For Ecol Manag 523:120480. https://doi.org/10.1016/j.foreco.2022.120480

Næsset E (2002) Predicting forest stand characteristics with airborne scanning laser using a practical two-stage procedure and field data. Remote Sens Environ 80:88–99. https://doi.org/10.1016/S0034-4257(01)00290-5

Näsi R, Honkavaara E, Lyytikäinen-Saarenmaa P, Blomqvist M, Litkey P, Hakala T, Viljanen N, Kantola T, Tanhuanpää T, Holopainen M (2015) Using UAV-based photogrammetry and hyperspectral imaging for mapping bark beetle damage at tree-level. Remote Sens 7:15467–15493. https://doi.org/10.3390/rs71115467

Näsi R, Honkavaara E, Blomqvist M, Lyytikäinen-Saarenmaa P, Hakala T, Viljanen N, Kantola T, Holopainen M (2018) Remote sensing of bark beetle damage in urban forests at individual tree level using a novel hyperspectral camera from UAV and aircraft. Urban for Urban Green 30:72–83. https://doi.org/10.1016/j.ufug.2018.01.010

Neto JC (2004) A combined statistical-soft computing approach for classification and mapping weed species in minimum-tillage systems (Doctoral dissertation). University of Nebraska—Linclon. Retrieved from https://digitalcommons.unl.edu/dissertations/AAI3147135

Nevalainen O, Honkavaara E, Tuominen S, Viljanen N, Hakala T, Yu X, Hyyppä J, Saari H, Pölönen I, Imai N, Tommaselli A (2017) Individual tree detection and classification with UAV-based photogrammetric point clouds and hyperspectral imaging. Remote Sens 9:185. https://doi.org/10.3390/rs9030185

Nezami S, Khoramshahi E, Nevalainen O, Pölönen I, Honkavaara E (2020) Tree species classification of drone hyperspectral and

RGB imagery with deep learning convolutional neural networks. Remote Sens 12:1070. https://doi.org/10.3390/rs12071070
Nuijten RJG, Coops NC, Watson C, Theberge D (2021) Monitoring the structure of regenerating vegetation using drone-based digital aerial photogrammetry. Remote Sens 13:1942. https://doi.org/10.3390/rs13101942
Onishi M, Ise T (2021) Explainable identification and mapping of trees using UAV RGB image and deep learning. Sci Rep 11:903. https://doi.org/10.1038/s41598-020-79653-9
Pádua L, Hruška J, Bessa J, Adão T, Martins L, Gonçalves J, Peres E, Sousa A, Castro J, Sousa J (2017) Multi-temporal analysis of forestry and coastal environments using UASs. Remote Sens 10:24. https://doi.org/10.3390/rs10010024
Panagiotidis D, Abdollahnejad A, Surový P, Kuželka K (2019) Detection of fallen logs from high-resolution UAV images. NZJFS. https://doi.org/10.33494/nzjfs492019x26x
Patacca M, Lindner M, Lucas-Borja ME, Cordonnier T, Fidej G, Gardiner B, Hauf Y, Jasinevičius G, Labonne S, Linkevičius E, Mahnken M, Milanovic S, Nabuurs G, Nagel TA, Nikinmaa L, Panyatov M, Bercak R, Seidl R, Ostrogović Sever MZ, Socha J, Thom D, Vuletic D, Zudin S, Schelhaas M (2023) Significant increase in natural disturbance impacts on European forests since 1950. Glob Change Biol 29:1359–1376. https://doi.org/10.1111/gcb.16531
Pedregosa F, Varoquaux G, Gramfort A, Michel V, Thirion B, Grisel O, Blondel M, Prettenhofer P, Weiss R, Dubourg V, Vanderplas J, Passos A, Cournapeau D, Brucher M, Perrot M, Duchesnay E (2011) Scikit-learn: machine learning in python. J Mach Learn Res 12(85):2825–2830
Polewski P, Yao W, Heurich M, Krzystek P, Stilla U (2015) Detection of fallen trees in ALS point clouds using a normalized cut approach trained by simulation. ISPRS J Photogramm Remote Sens 105:252–271. https://doi.org/10.1016/j.isprsjprs.2015.01.010
Polewski P, Shelton J, Yao W, Heurich M (2021) Instance segmentation of fallen trees in aerial color infrared imagery using active multi-contour evolution with fully convolutional network-based intensity priors. ISPRS J Photogramm Remote Sens 178:297–313. https://doi.org/10.1016/j.isprsjprs.2021.06.016
Qin H, Zhou W, Yao Y, Wang W (2022) Individual tree segmentation and tree species classification in subtropical broadleaf forests using UAV-based LiDAR, hyperspectral, and ultrahigh-resolution RGB data. Remote Sens Environ 280:113143. https://doi.org/10.1016/j.rse.2022.113143
Ramalho De Oliveira LF, Lassiter HA, Wilkinson B, Whitley T, Ifju P, Logan SR, Peter GF, Vogel JG, Martin TA (2020) Moving to automated tree inventory: comparison of UAS-derived lidar and photogrammetric data with manual ground estimates. Remote Sens 13:72. https://doi.org/10.3390/rs13010072
Rhodes MW, Bennie JJ, Spalding A, ffrench-Constant RH, Maclean IMD (2022) Recent advances in the remote sensing of insects. Biol Rev 97:343–360. https://doi.org/10.1111/brv.12802
Safonova A, Hamad Y, Alekhina A, Kaplun D (2022) Detection of Norway spruce trees (Picea Abies) infested by bark beetle in UAV images using YOLOs architectures. IEEE Access 10:10384–10392. https://doi.org/10.1109/ACCESS.2022.3144433
Sun Z, Wang X, Wang Z, Yang L, Xie Y, Huang Y (2021) UAVs as remote sensing platforms in plant ecology: review of applications and challenges. J Plant Ecol 14:1003–1023. https://doi.org/10.1093/jpe/rtab089
Sun Y, Jin X, Pukkala T, Li F (2022) Predicting individual tree diameter of larch (Larix olgensis) from UAV-LiDAR data using six different algorithms. Remote Sens 14:1125. https://doi.org/10.3390/rs14051125
Suomalainen J, Oliveira RA, Hakala T, Koivumäki N, Markelin L, Näsi R, Honkavaara E (2021) Direct reflectance transformation methodology for drone-based hyperspectral imaging. Remote Sens Environ 266:112691. https://doi.org/10.1016/j.rse.2021.112691
Thiel C, Mueller MM, Epple L, Thau C, Hese S, Voltersen M, Henkel A (2020) UAS imagery-based mapping of coarse wood debris in a natural deciduous forest in Central Germany (Hainich National Park). Remote Sens 12:3293. https://doi.org/10.3390/rs12203293
Tucker CJ (1979) Red and photographic infrared linear combinations for monitoring vegetation. Remote Sens Environ 8:127–150. https://doi.org/10.1016/0034-4257(79)90013-0
Turkulainen E, Honkavaara E, Näsi R, Oliveira RA, Hakala T, Junttila S, Karila K, Koivumäki N, Pelto-Arvo M, Tuviala J, Östersund M, Pölönen I, Lyytikäinen-Saarenmaa P (2023) Comparison of deep neural networks in the classification of bark beetle-induced spruce damage using UAS images. Remote Sens 15:4928. https://doi.org/10.3390/rs15204928
Vincini M, Frazzi E, D'Alessio P (2008) A broad-band leaf chlorophyll vegetation index at the canopy scale. Precision Agric 9:303–319. https://doi.org/10.1007/s11119-008-9075-z
Wermelinger B (2004) Ecology and management of the spruce bark beetle *Ips typographus*—a review of recent research. For Ecol Manag 202:67–82. https://doi.org/10.1016/j.foreco.2004.07.018
Woebbecke DM, Meyer GE, Von Bargen K, Mortensen DA (1995) Color indices for weed identification under various soil, residue, and lighting conditions. Trans ASAE 38:259–269. https://doi.org/10.13031/2013.27838
Wu C, Niu Z, Tang Q, Huang W (2008) Estimating chlorophyll content from hyperspectral vegetation indices: modeling and validation. Agric for Meteorol 148:1230–1241. https://doi.org/10.1016/j.agrformet.2008.03.005
Wu B, Liang A, Zhang H, Zhu T, Zou Z, Yang D, Tang W, Li J, Su J (2021) Application of conventional UAV-based high-throughput object detection to the early diagnosis of pine wilt disease by deep learning. For Ecol Manag 486:118986. https://doi.org/10.1016/j.foreco.2021.118986
Yang C, Everitt JH, Bradford JM, Murden D (2004) Airborne hyperspectral imagery and yield monitor data for mapping cotton yield variability. Precis Agric 5:445–461. https://doi.org/10.1007/s11119-004-5319-8
Yu R, Luo Y, Li H, Yang L, Huang H, Yu L, Ren L (2021) Three-dimensional convolutional neural network model for early detection of pine wilt disease using UAV-based hyperspectral images. Remote Sens 13:4065. https://doi.org/10.3390/rs13204065
Zakrzewska A, Kopeć D, Ochtyra A, Potůčková M (2023) Can canopy temperature acquired from an airborne level be a tree health indicator in an urban environment? Urban for Urban Green 79:127807. https://doi.org/10.1016/j.ufug.2022.127807

Publisher's Note Springer Nature remains neutral with regard to jurisdictional claims in published maps and institutional affiliations.